Advances in Applied Energy 2 (2021) 100010

Contents lists available at ScienceDirect

Advances in Applied Energy

journal homepage: www.elsevier.com/locate/adapen

Low-carbon hydrogen via integration of steam methane reforming with molten carbonate fuel cells at low fuel utilization

Stefano Consonni[a,b,1], Luca Mastropasqua[c,1,*], Maurizio Spinelli[b], Timothy A. Barckholtz[d], Stefano Campanari[a]

[a] Politecnico di Milano, Department of Energy, Via Lambruschini 4, Milan 20156, Italy
[b] LEAP scarl, via Nino Bixio 27C, Piacenza 29121, Italy
[c] Advanced Power and Energy Program, University of California, Irvine, CA 92697, USA
[d] ExxonMobil Research and Engineering - 1545 Route 22 East, Annandale, NJ 08801, USA

ARTICLE INFO

Keywords:
Molten carbonate fuel cell
Steam methane reforming
Retrofit
Carbon capture and storage
Hydrogen

ABSTRACT

Hydrogen production is critical to many modern chemical processes – ammonia synthesis, petroleum refining, direct reduction of iron, and more. Conventional approaches to hydrogen manufacture include steam methane reforming and autothermal reforming, which today account for the lion's share of hydrogen generation. Without CO_2 capture, these processes emit about 8.7 kg of CO_2 for each kg of H_2 produced. In this study, a molten carbonate fuel cell system with CO_2 capture is proposed to retrofit the flue gas stream of an existing Steam Methane Reforming plant rated at 100,000 $Nm^3\ h^{-1}$ of 99.5% pure H_2. The thermodynamic analysis shows direct CO_2 emissions can be reduced by more than 95%, to 0.4 to 0.5 kg CO_2/kg H_2, while producing 17% more hydrogen (with an increase in natural gas input of approximately 37%). Because of the additional power and hydrogen generation of the carbonate fuel cell, the efficiency debit associated with CO_2 capture is quite small, reducing the SMR efficiency from 76.6% without capture to 75.6% with capture. In comparison, the use of standard amine technology for CO_2 capture reduces the efficiency below 70%. This demonstrates the synergistic nature of the carbonate fuel cells, which can reform natural gas to H_2 while simultaneously capturing CO_2 from the SMR flue gas and producing electricity, giving rise to a total system with very low emissions yet high efficiency.

1. Introduction

The International Energy Agency (IEA)'s estimates of world primary energy demand in 2040 predict a fossil fuel share (i.e., coal, oil and gas) of 74% in the "New Policies" scenario and 58% in the "450 Scenario" [1]. Oil and gas only are expected to cover 51% and 45% of total primary energy demand, respectively. Renewables account for the balance of the primary energy demand, and include solar, wind, nuclear, hydro, and biomass, and – as a group – are a growing proportion of the primary energy supply. Likewise, the energy carriers of the future are moving away from petroleum-based products for transportation and towards electricity and biofuels. A much-discussed alternative fuel is hydrogen [2,3], which – when made from renewable power and electrolysis – is often labelled "green" hydrogen. Hydrogen generated from fossil fuels is usually referred to as "grey" hydrogen, as there will be greenhouse gas emissions associated with its production. When CO_2 capture and sequestration is added to the fossil generation, hydrogen is referred to as "blue" hydrogen. This work will focus on the production of "blue" hydrogen and the development of integrated technologies for capturing CO_2. On the other hand, CO_2 transport, storage and sequestration or utilization technologies, despite being an essential step in the carbon cycle to achieve the low-carbon standards of the produced hydrogen, will not be addressed in this work.

A wide variety of methods to produce "blue" hydrogen have been suggested in the literature, each with its own advantages and challenges [4,5]. Abe et al. [3] summarize the potentialities and obstacles of using hydrogen as a sustainable energy carrier, especially focusing on the challenges associated with its storage in gaseous, liquid or solid form. Nikolaidis et al. [6] compare 14 different hydrogen production methods, both conventional and renewable, from an energy efficiency and economic perspective. Parkinson et al. [7] presented a comparative framework to assess the techno-economic performance of hydrogen production methods, including hydrocarbon reforming with CCS. Khojasteh Salkuyeh et al. [8] studied the life cycle analysis of four different hydrogen production technologies using natural gas as feedstock, finding a scenario where a carbon price as low as $5/ton CO_2 can be sufficient for cost breakeven with conventional SMR plants.

* Corresponding author.
E-mail address: lm1@apep.uci.edu (L. Mastropasqua).
[1] These authors have contributed equally to this work.

https://doi.org/10.1016/j.adapen.2021.100010
Received 3 February 2021; Received in revised form 4 February 2021; Accepted 4 February 2021
Available online 10 February 2021

Nomenclature

Symbols

$\eta_{el,total}$	total net electric efficiency / %
$\eta_{el,MCFC}$	MCFC net electric efficiency / %
$\eta'_{el,total}$	adjusted total net electric efficiency / %
$\eta'_{el,MCFC}$	adjusted MCFC net electric efficiency / %
$\eta_{H_2,total}$	total hydrogen efficiency / %
$\eta'_{H_2,total}$	adjusted total hydrogen efficiency / %
$\eta_{H_2,MCFC}$	MCFC net hydrogen efficiency / %
$\eta'_{H_2,MCFC}$	adjusted MCFC net hydrogen efficiency / %
$\eta_{el+H_2,total}$	total first law net efficiency / %
$\eta_{el+H_2,MCFC}$	MCFC first law net efficiency / %
e_i	specific emissions of component i / kg GJ^{-1}
E_i	emissions of component i / kg s^{-1}
$\dot{Q}_i$	chemical energy flow rate in stream i / MW_{th}
SPECCA	specific primary energy consumption for CO_2 avoided / MJ kg_{CO2}^{-1}
S/C	steam-to-carbon ratio / -
U_f	fuel utilization factor / -
U_{CO_2}	CO_2 utilization factor / -
U_{ox}	oxidant utilization factor / -
$\dot{W}$	power production / MW_e
x_i	molar fraction of chemical species i, / -

Acronyms

AC	activated carbons
CCS	carbon capture and storage
CHP	combined heat and power
GPU	gas processing unit
LHV	lower heating value
MCFC	molten carbonate fuel cell
MDEA	methyl-di-ethanolamine
MEA	mono-ethanolamine
NGCC	natural gas combined cycle
NG	natural gas
FTR	fired tubular reactor
PSA	pressure swing adsorption
SMR	steam methane reformer
S+M+C	SMR with MCFC and CO_2 capture
LT-WGS	low temperature water gas shift
MT-WGS	medium temperature water gas shift
HT-WGS	high temperature water gas shift

Subscripts/superscripts

ref	reference system without CCS
an	anode-side
cat	cathode-side
p	primary energy

Diverse technologies have been explored to achieve the production of low-carbon hydrogen from steam methane reforming. The most prominent post-combustion technologies under investigation are: i) chemical adsorption via amines (MDEA, MEA) [9,10]; ii) oxy-fuel combustion [11,12]; and iii) solid sorbents in chemical looping reactors [13–16]. Collodi et al. [9] proposed a comparative techno-economic analysis of different configurations using chemical adsorption (MDEA, MEA), ionic membranes and cryogenic separation carbon capture. Consonni et al. [10] investigated the thermodynamic performance of auto-thermal reformers and fired tubular reactors for large-scale steam reforming with amines capture for low-carbon hydrogen and electricity production. Herraiz et al. [17] have recently studied sequential combustion in SMR plants for reducing capital and operating costs by using a single MEA process for CO_2 capture from both the hydrogen process and power production plant. Sanusi et al. [11,12] studied a low-carbon hydrogen production plant using steam methane reforming reactor integrated with an ion-transport membrane reactor that produces the oxygen required to an oxy-fuel combustor. Following their optimization, they found an overall plant efficiency of 59.4% and an annualized cost of hydrogen of $12/GJ. Martinez et al. [13] presented a novel sorption enhanced Ca/Cu chemical looping process for hydrogen production able to achieve 77% hydrogen production efficiencies with a 94% carbon capture ratio. Diglio et al. [14] reported another sorption enhanced steam methane reforming reactor employing a novel material with CaO/CuO/Al_2O_3(NiO) pellets. They showed a methane conversion of 95% with a 3.2 mol_{H2} mol_{CH4}^{-1} hydrogen yield. Their techno-economic analysis reported the possibility of reaching an investment pay-back period of 2.2 years when the hydrogen in used in a downstream solid oxide fuel cell system.

This study focuses on an electrochemical route to generate "blue" hydrogen: the retrofit of Steam Methane Reformers (SMR) with Molten Carbonate Fuel Cells (MCFCs) with CO_2 capture. A recent review [18] highlights the potential for the use of carbonate fuel cells for CO_2 capture. MCFCs have the rather unique feature of conducting CO_3^{2-} ions and thus concentrating the CO_2 into the anode compartment. Besides being electrochemically active, MCFCs can activate heterogenous catalytic reactions such as Steam Methane Reforming and Water Gas Shift (WGS) within the porous micro-structure of the electrodes. Natural gas supplied to the anode compartment undergoes steam reforming and WGS, converting methane into H_2 and CO in an indirect internal reforming layer heated by groups of adjacent cells. At the same time, H_2 is electro-oxidised with CO_3^{2-} ions coming from the cathode-side compartment. Eqs. (1)–(6) report the main anode-side and cathode-side catalytic and electrochemical reactions:

Pre-reforming reactions:

$$CH_4 + H_2O \rightleftarrows 3H_2 + CO \quad (\Delta H_r = 206 \text{ kJ mol}^{-1}) \tag{1}$$

$$CO + H_2O \rightleftarrows H_2 + CO_2 \quad (\Delta H_r = -41 \text{ kJ mol}^{-1}) \tag{2}$$

Anode-side reactions:

$$\boldsymbol{H_2 + CO_3^{2-} \rightarrow H_2O + CO_2 + 2e^-} \tag{3}$$

$$CH_4 + H_2O \rightleftarrows 3H_2 + CO \quad (\Delta H_r = 206 \text{ kJ mol}^{-1}) \tag{4}$$

$$CO + H_2O \rightleftarrows H_2 + CO_2 \quad (\Delta H_r = -41 \text{ kJ mol}^{-1}) \tag{5}$$

Cathode-side reactions:

$$CO_2 + \frac{1}{2}O_2 + 2e^- \rightarrow CO_3^{2-} \tag{6}$$

From a carbon capture standpoint, the electrochemical reactions given by Eqs. (3) and (6) are crucial to transport CO_2 from the cathode-side to the anode-side, thus concentrating CO_2 into the stream exiting the anode. The basic driver of this process is hydrogen, which is generated by the reactions in Eqs. (4) and (5). For the application considered here, where both CO_2 capture and H_2 production are relevant, the cell operating conditions should be adjusted to maximize the capture of CO_2 and maximize the generation of hydrogen.

The literature on the use of MCFCs as post-combustion CO_2 capture systems for power plants and industrial sources is broad and well-established [19]. Specifically, Sagiura et al. [20] conducted an experimental study using an 81 cm^2 cell with a lithium/sodium mixture electrolyte and evaluated the variation in voltage performance at different p_{O2}/p_{CO2} and p_{H2O} at cathode inlet. They verified that their cell was able to provide a 24% CO_2 removal efficiency from a flue gas stream of a combined cycle system. Similarly, Lusardi et al. [21] studied different configurations for retrofitting a gas turbine cycle with an MCFC, verifying that these cells are able to operate as CO_2 concentrators achieving volume fraction of 51-81% at the anode outlet. Other authors proposed the operation of MCFC for CO_2 separation from lignite flue gases [22].

Recently, experimental studies have been reported on MCFCs at very deep CO_2 capture, showing that a new fuel cell chemistry plays a role when the CO_2 concentration drops below about 0.5% concentration in the cathode [23]. Some of the authors of this work have also investigated MCFC retrofit from natural gas power plants [24,25], from coal plants [26] and from industrial applications such as cement [27] and steel [28].

In parallel to developing MCFC systems for CCS applications, the literature has proposed employing MCFCs for the co-production of multiple useful energy products, such as electricity, hydrogen, cooling, and heat. Margalef et al. [29] studied the use of MCFC for tri-generation application in the hydrogen supply chain, comparing high temperature fuel cells for hydrogen generation to more conventional distributed or centralized SMR. Moradpoor et al. [30] proposed a system integration of an MCFC combined with a Stirling engine and a Kalina cycle to co-produce cooling, heating and power. Mehrpooya et al. [31] introduced a hybrid multi-generation MCFC system integrated with cryogenic CO_2 capture and an ammonia-water absorption refrigeration cycle to co-produce electricity, heat and cooling power. Agll et al. [32] reports the case study of a combined heat, hydrogen and power MCFC system supplied by various biogenic feedstock to power a university campus. Li et al. [33] performed a techno-economic analysis for a MCFC tri-generation system for commercial building applications, such as grocery and retail businesses. They showed that the tri-generation system can be economically competitive and can reduce CO_2 emissions by 10-44% even with natural gas as feedstock. Rinaldi et al. [34], investigate different configurations of an MCFC tri-generation system supplied with biogas feedstock to recover CO_2 from an internal combustion engine flue gas stream. They investigated multiple MCFC in series and calculated a maximum carbon capture ratio of 90% with three MCFC in series.

The background described above does not exhaust the realm of appealing MCFC-based concepts. More specifically, no publication appears to have addressed the thermodynamic performance and greenhouse gases emission benefits achievable by retrofitting a Fired Tubular Reformer (FTR) with an MCFC-based system that, in addition to the co-production of electricity and hydrogen, can give dramatic reductions of CO_2 emissions. This paper investigates this option for the operating conditions typical of a large-scale steam reformer (rated at 106,000 Nm^3/h of 99.999% pure H_2), showing how a substantial system integration redesign is required compared to other MCFC systems for power generation or other co-generation systems. Moreover, the paper assesses for the first time the greenhouse gas reduction benefits associated with the use of an electrochemical CCS system in a steam methane reformer. In summary, this work features the following novel contributions:

- Thermodynamic review of a commercial reference MCFC system for power and heat co-production
- Assessment of a reference FTR performance and CO_2 emissions
- Formulation of a novel co-generative MCFC retrofit for the combined production of electricity and hydrogen with CO_2 capture
- Discussion of design choices for the operation of the MCFC at low fuel utilization factor and for CO_2 and hydrogen recovery
- Assessment of benefits (and caveats) of operating the MCFC at low fuel utilization factors
- Evaluation of thermodynamic performance, direct and indirect CO_2 emissions for three retrofit scenarios, with comparisons to the reference SMR plant

In the following, Section 2 illustrates the methodology, the reference MCFC and SMR systems, the proposed plant configuration, and the rationale of our analysis. The performance of the baseline FTR is taken as the reference to assess the proposed SMR+MCFC system with CO_2 capture via appropriately defined key performance indicators. Section 3 summarises the main results in terms of operating conditions, overall thermodynamic performance, direct and equivalent greenhouse gas emissions.

Table 1
Thermodynamic performance and CO_2 emissions of the reference CHP stack without CCS.

Parameter	Unit	Value
Fuel input (LHV)	kW	644.26
FC net power	kW	315.05
Aux power	kW	-11.23
Net power	kW	303.82
Electrical fficiency (LHV)	%	47.16
CO_2 emissions	kg CO_2 MWh_{el}^{-1}	437.36

2. Methodology and scope

2.1. Simulation tools and main assumptions

Mass and energy balances are evaluated by the modular simulation code “GS” originally conceived at Princeton University [35] and further developed at the Department of Energy of Politecnico di Milano [36]. The application to MCFC-based systems has been validated for a number of retrofit CCS solutions [26].

2.2. Reference MCFC plant without CCS

To establish a reference for the systems with CO_2 capture analysed in this paper, we have modelled the commercial plant developed by the main MCFC manufacturer nowadays on the market [37,38]. The system is rated at 1.4 MW_{el} (AC net) and is comprised of four identical stacks each generating a gross DC power of approximately 375 kW_{el}. A simplified layout of the reference system is shown in Fig. 1.

This system is modelled and simulated in nominal operating conditions, giving the thermodynamic performance summarized in Table 1. Table A1 reports the thermodynamic conditions of each flow in Fig. 1. After accounting for losses and auxiliaries, we estimate that each stack gives 338 kW_{el} (AC), for a total plant net AC power of the whole 4-stack module of 1.35 MW_{el} and a net LHV efficiency of nearly 47.2%.

The commercial system is designed for cogeneration purposes, with no provisions for a separation and purification of CO_2. The CO_3^{2-} ion that goes through the electrolyte from the cathode to the anode turns to CO_2 at the anode. Then, CO_2 and unoxidised fuel species (H_2 and CO) are sent to the catalytic burner, producing a carbon loop among the cathode, the anode, and the catalytic oxidiser, which can be seen in the flow diagram reported in Fig. 2. The carbon dioxide eventually emitted originated in the carbon fuel fed to the plant as natural gas.

2.3. Reference FTR

Fig. 3 depicts the configuration of the conventional Steam Methane Reformer (SMR) taken as the reference or baseline case, which is a revised version of the Fired Tubular Reactor (FTR) plant already modelled by some of the authors in [10]. Plant capacity is 106,000 $Nm^3\ h^{-1}$ (291.3 MW LHV) of hydrogen at 99.999% purity.

The FTR plant converts the natural gas feed into hydrogen-rich syngas via endothermic steam-methane reforming sustained by the combustion, in air, of a fraction of the inlet natural gas and recycled process gas. In the reference FTR considered here reforming takes place at 850°C, 25 bar, with a steam-to-carbon ratio (S/C) equal to 3.0. Natural gas at 33 bar and ambient temperature is first desulphurised and then split into a feed stream for reforming and a stream for combustion in the FTR furnace. The air-to-fuel ratio of the FTR burners is set to give 1% oxygen (by volume) in the flue gases, whereby the concentration of CO_2 in flue gases is approximately 21% by volume.

The fuel and steam processing island features two main heat recovery sections: i) a section where heat recovered from flue gases is used to generate superheated steam (48 bar, 400°C) and pre-heat the air and natural gas upstream of the FTR furnace; ii) a section where heat recovered

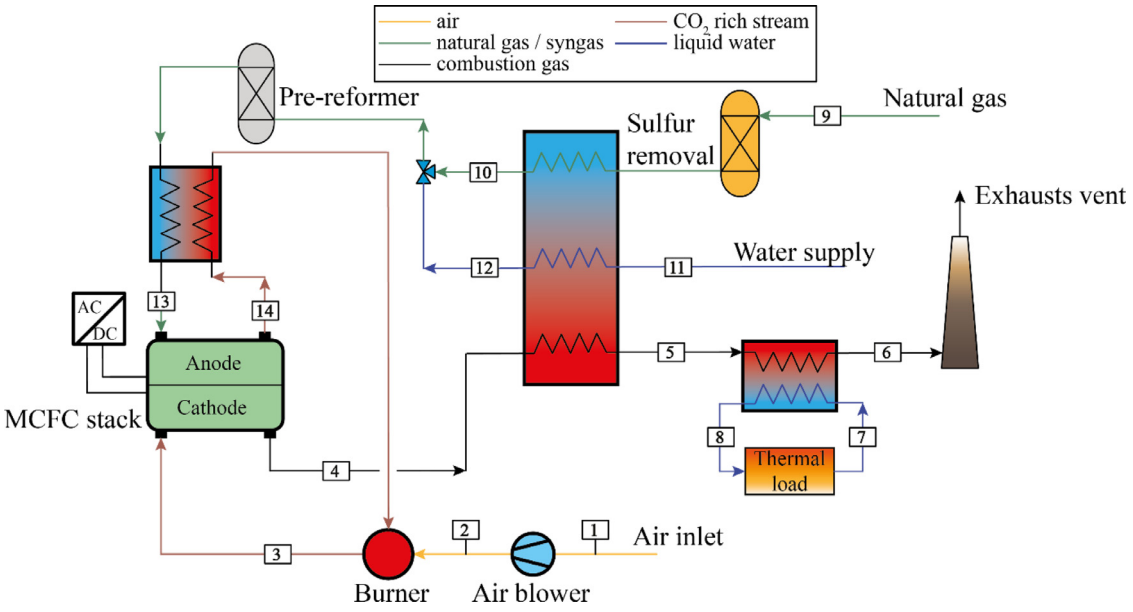

Fig. 1. Simplified layout of the reference CHP system without CCS.

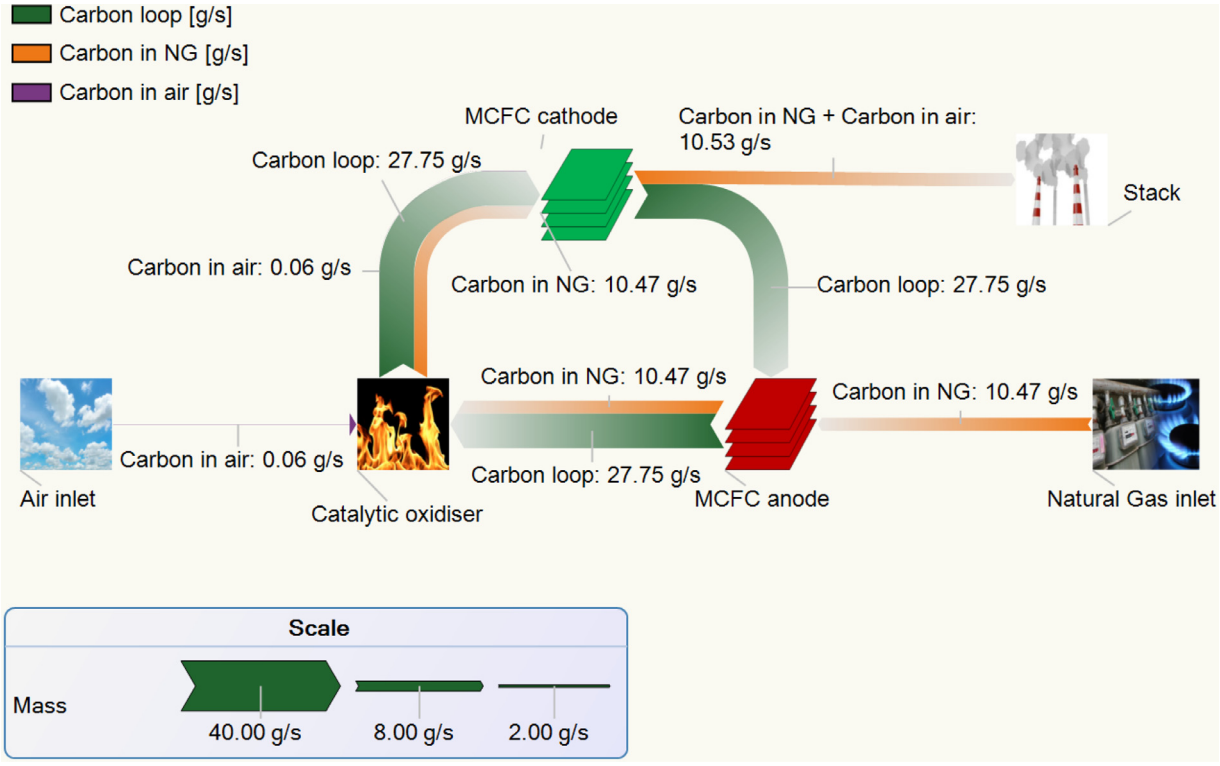

Fig. 2. Carbon flow diagram of the reference 1.4 MW_e CHP plant.

from the hydrogen-rich stream generated in the FTR is used to generate additional superheated steam. The latter includes a Medium Temperature Water Gas Shift (MT-WGS) reactor operating at 320°C where most of the CO left in the stream exiting the FTR is converted into CO_2 with further generation of H_2. The plant also comprises a pre-reforming reactor, where most hydrocarbons heavier than methane are reformed to reduce the risk of coking in the FTR, and a Pressure Swing Adsorption (PSA) unit for purification of hydrogen.

The superheated steam generated in the heat recovery sections feeds a steam turbine that produces a power nearly equal to the auxiliary power consumption of the whole plant, so that there is no electric power import nor export. Steam for reforming is bled from the High-Pressure Turbine at 31 bar and 347°C and is mixed with desulfurized natural gas at 380°C and 28 bar.

Overall performance and greenhouse gas emissions are summarized in Table 2: The net hydrogen production efficiency (106,090 $Nm^3\ h^{-1}$

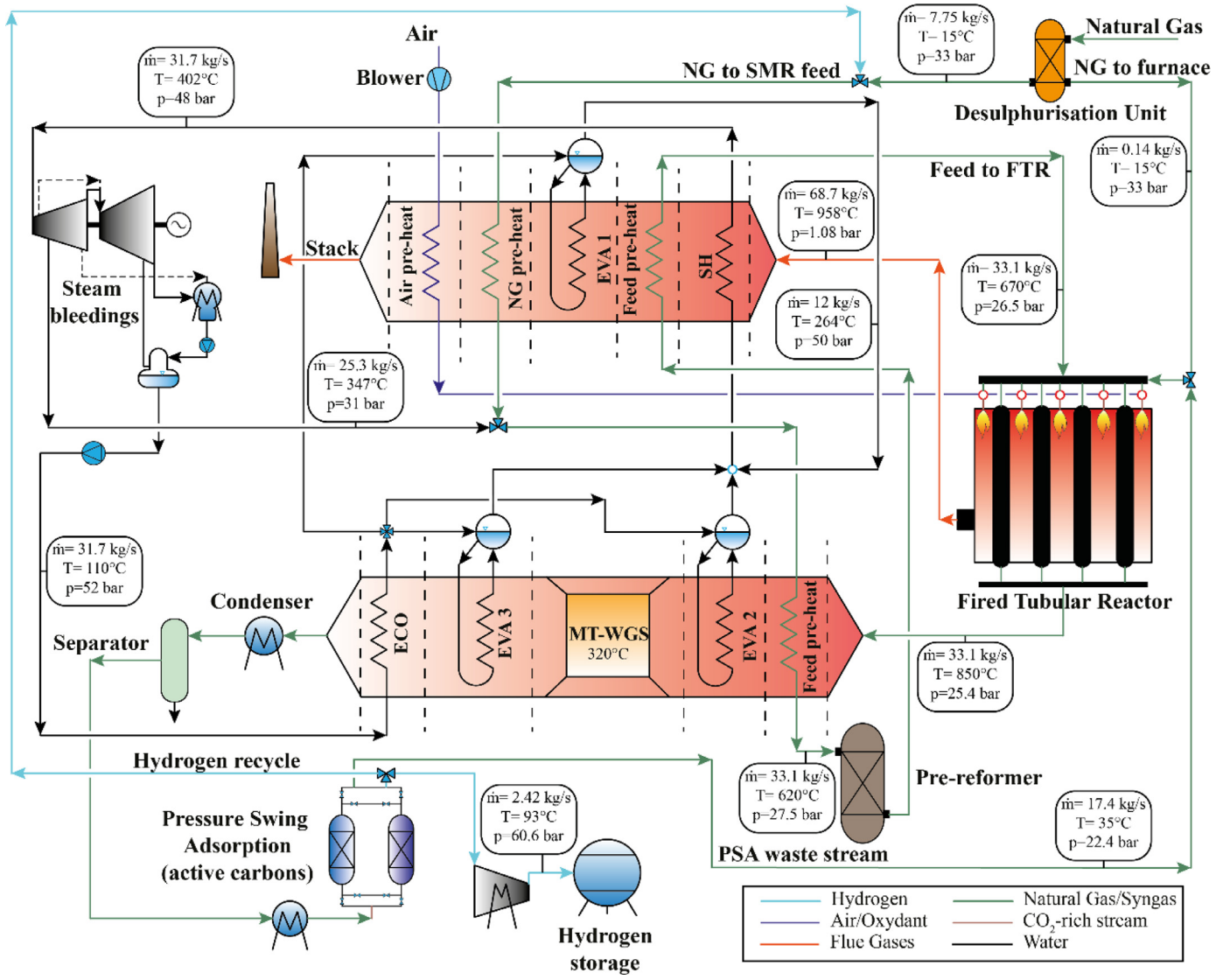

Fig. 3. Reference SMR plant with Fired Tubular Reactor (FTR).

Table 2
Overall thermodynamic and greenhouse gas emission performance of the reference FTR without CCS.

	Unit	Value
NG inlet to SMR (LHV)	MW	380.3
Net H_2 from SMR	MW ($Nm^3\ h^{-1}$)	291.3 (106,089.8)
Steam cycle gross power	MW	6.1
Aux power	MW	-6.1
Net Power	MW	0.04
H_2 efficiency	%	76.6
First law efficiency (LHV)	%	76.6
CO_2 emissions	kg CO_2 kg H_2^{-1}	8.7
CO_2 emissions	kg CO_2 GJ H_2^{-1}	72.2

of H_2 with LHV 119.95 MJ kg^{-1}, i.e., 291.3 MW_{LHV}) is 76.6% based on the natural gas LHV input. The specific CO_2 emissions result are 72.2 kg of CO_2 per GJ_{LHV} of hydrogen or 8.7 kg of CO_2 per kg of H_2.

2.4. System integration

This work aims at assessing technical issues and performance of retrofitting an SMR plant, such as the reference FTR described in Section 2.3, with a MCFC-based system adapted from that presented in Section 2.2. The goals of the retrofit are twofold:

i) abate the CO_2 emissions associated with the production of hydrogen of the existing SMR;
ii) increase hydrogen production capacity (without a significant increase of CO_2 emissions).

As a third, but more minor benefit, the substantial power output of the MCFC needed for CO_2 capture makes the SMR+MCFC combination a net exporter of electric power and increases the overall value proposition of the resulting integrated plant.

The following section describes the proposed retrofit configuration, while Table 3 reports the main assumptions adopted in the simulations.

The biggest localized source of CO_2 emitted by the SMR is in the flue gases, where the combustion of natural gas and the PSA tail-gas gives a CO_2 concentration of approximately 21% by volume [9]. In the retrofit envisaged here, the SMR flue gases are fed to the cathode compartment of the MCFC after being pre-heated to 575°C (point #8 of Fig. 4 and Table A2). The anode compartment is fed with additional natural gas (point #13), which must be appropriately desulphurised to meet MCFC specifications. The MCFC system is arranged in modules of stacks, similar to the configuration in Section 2.2.

Table 3
Main assumptions adopted to evaluate operating conditions and performances of the proposed retrofit of an SMR with the MCFC system with carbon capture.

Parameter	Unit	Value
Ambient conditions		
Temperature	°C	15
Pressure	bar	1.0132
Relative humidity	%	60
Natural gas properties		
Composition	%	CH_4 95.0; C_2H_6 3.0; N_2 2.0
LHV	MJ kg^{-1}	48.196
MCFC		
Inlet temperature cathode	°C	575.0
Inlet temperature internal pre-reformer	°C	450.0
Inlet temperature anode	°C	600.0
Maximum cathodic ΔT across cell [°C]	°C	70.0
Minimum xO_2 cathode outlet	%	2.5
Minimum xCO_2 cathode outlet	%	1.0
Minimum cell voltage	mV	650.0
Air/fuel channels pressure losses	%	2.0
DC/AC electrical efficiency	%	97.0
Heat loss	% on LHV at inlet	1.0
External pre-reformer		
Inlet temperature	°C	450.0
S/C ratio at inlet	-	2.2
Ethane conversion	%	100.0
Methane conversion	%	2.5
Heat exchangers		
Hot and cold side $\Delta p/p_{in}$	%	2.0
Heat Losses	% of heat transferred	1.0
Sub-cooling in economiser	°C	6.0
ΔT_{min} in gas-water heat exchangers	°C	15.0
ΔT_{min} in gas-gas heat exchangers	°C	30.0
Chemical reactors		
HT-WGS inlet temperature	°C	340
LT-WGS inlet temperature	°C	180
WGS advancement of reaction	%	0.90
Pressure losses $\Delta p/p_{in}$	%	3.0
Desulphurization unit inlet temperature	°C	15.0
Pressure swing adsorption		
Minimum regeneration pressure	bar	1.0
Column diameter	m	3.0
Column height	m	15.0
Cycle time	s	1000
Activated carbons (AC) density	kg m^{-3}	850 [39]
Zeolite LiX density	kg m^{-3}	2400 [39]
AC-to-zeolite volume ratio	%	60.0
Miscellaneous		
Minimum exhaust temperature at stack	°C	80.0
Blower isentropic efficiency	%	80.0
Blower mechanical-electrical efficiency	%	94.0
Hydrogen pressure for export	bar	60.0
Hydrogen purity for export	%	99.999
GPU specific electric consumption	kJ $kgCO_2^{-1}$ *	variable

* based on CO_2 to storage (excluded PSA compressor consumption).

As reported in Table 3, the operating conditions of the MCFC are subjected to a number of constraints, which we assumed to be: a minimum voltage of 650 mV, a maximum ΔT across the cathode (70°C), a minimum oxygen content (2.5% molar) and a minimum CO_2 content (1% molar) at the cathode outlet. The minimum operating voltage of 650 mV is chosen to maintain a high electrical efficiency in the stack and avoid potential complications, such as corrosion. The temperature rise across the fuel cell is required to avoid temperature runaways and maintain materials performance, as described in the literature [40]. The last two (minimum O_2 and CO_2 content at cathode outlet) follow from the recent observations by Rosen et al. [23] who showed that at very low CO_2 concentrations hydroxide ions can be formed in the cathode and transported to the anode. Thus, we have limited the cathode exit concentration to a minimum of 1% to avoid this complication.

Air can also be fed between the SMR furnace and the cathode inlet stream and mixed with the inlet flue gases to control the cathode O_2 inlet concentration. In this application, the air stream (point #4) is substantial because the flue gases from the SMR are characterized by

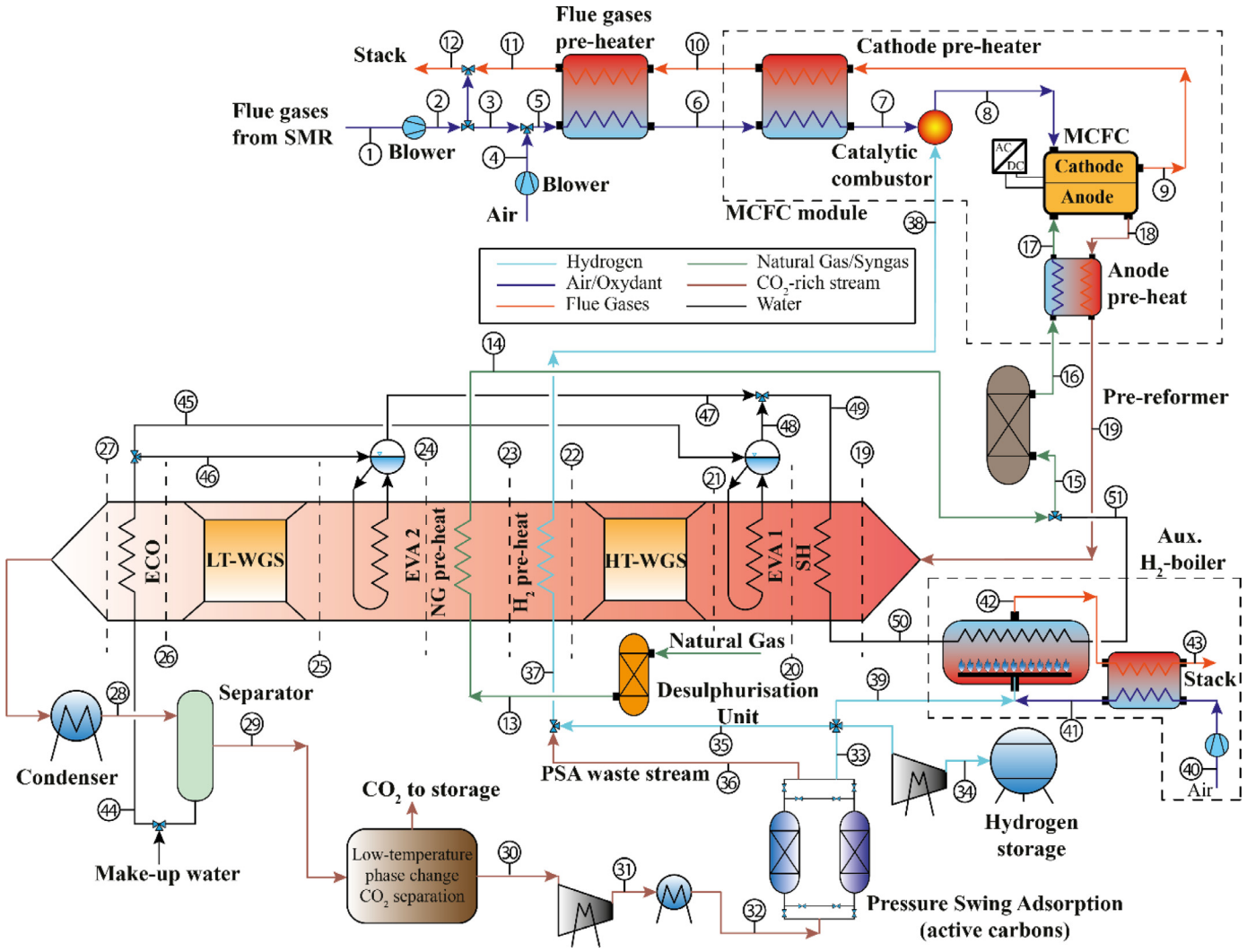

Fig. 4. Retrofit layout for post-combustion capture with MCFCs from a SMR plant. The auxiliary H_2-boiler section contained in the dashed box is necessary only for operation at $U_f = 45\%$, due to the need of obtaining the required steam temperature at stream #51. This is not necessary at higher U_f, due to the higher exothermicity of the fuel cell.

a low O_2 concentration (i.e., 1%). Therefore, air is necessary to obtain a sufficiently high O_2 concentration prior entering the catalytic oxidiser and the cathode inlet, as required by the cathode chemistry (Eq. (6)).

Unlike conventional applications, where the fuel cell is used just to generate power and possibly heat, in the retrofit considered here the production of power is an ancillary outcome. In fact, in our case the most valuable outcomes are CO_2 capture and the increase of hydrogen production capacity. Rather than pushing fuel utilization to enhance power output and electrical efficiency, in this analysis we consider a range of relatively low fuel utilization factors to increase the production of hydrogen at the expense of less power output. The requirements and the implications of this type of operation are discussed in the following, where we compare the operation with fuel utilization factors of 45%, 60% and 75%, the last one being near the conventional operating condition reported in Section 2.1.

2.5. Low fuel utilization factors

Operation at low utilization factors entails atypical conditions for the cell. Unlike in the case of high fuel utilization, the cell may become endothermic as the reaction enthalpy of the reforming reactions (Eq. (4)) overcomes the heat made available by the exothermic electrochemical oxidation of hydrogen. When this happens, the highest temperature in the stack is reached at the anode/cathode inlet rather than at their outlet, and the common practice of fully pre-heating the reactant streams to the anode and the cathode with the flows exiting the cell becomes unfeasible. To pre-heat the reactants to an appropriate temperature level (i.e., 600-650°C) we have explored the following options.

1 Introduce an additional catalytic oxidiser upstream of the cathode inlet and use the stream exiting the oxidiser to heat the stream of reactants both upstream and downstream of the pre-reforming reactor.
The major issues raised by this option are (i) feasibility of catalytic oxidation at the expected temperature and oxygen content; (ii) hazard generated by the need to transfer heat from a stream with a significant content of oxygen (the flow fed to the cathode) to the fuel stream entering the pre-reformer and the anode. A possible workaround to the second issue would be the introduction of an intermediate heat transfer loop with an inert fluid with favourable thermal properties, such as supercritical CO_2, which however would entail significant complications of the heat exchange network and critical operating conditions. For these reasons, throughout our analysis we do not consider any heat transfer between fuel streams and oxygen-bearing streams.

2 Adopt a non-adiabatic pre-reforming reactor where heat released by the flue gases exiting a catalytic oxidiser placed on the cathode side is transferred to the stream being pre-reformed. The major downsides of this option are the feasibility of such an unconventional component like a non-adiabatic pre-reformer and the fuel consumption of the catalytic oxidiser.
3 Substitute the pre-reforming guard bed with a Catalytic Partial Oxidation (CPO) guard bed. CPO reactors are used in fuel cell systems as fuel pre-processors to produce a syngas rich in CO and H_2 to be supplied to the cell anode. In this case the oxidation of a fraction of the hydrocarbon feedstock provides the heat needed to bring the anode reactants to the appropriate thermal level without the need for process water, which greatly simplifies the heat exchange network to produce steam.
The main challenge of this option is the feasibility of CPO reactors operated with stoichiometric or sub-stoichiometric oxygen feed. The syngas produced by the CPO reactor should not contain any non-reacted oxygen, while the literature reports that CPO reactors are operated with high oxygen excess [41].

The layout considered here and reported in Fig. 4 adopts a somewhat "safer" version of option 1, with a catalytic oxidiser that pre-heats the cathode inlet stream, while the anode inlet stream is moderately pre-heated to 450°C by heat exchange against the anode outlet stream. By avoiding the heat transfer from oxygen-bearing streams and fuels streams, such configuration greatly reduces explosion/fire hazards.

With very low fuel utilization factors (U_f below approximately 45%) the heat capacity of the anode outlet stream is not enough to pre-heat, evaporate and superheat the steam needed for the pre-reforming reactor. To make up this shortfall of heat and steam in these cases, we have assumed that a fraction of the hydrogen exiting the PSA system is combusted in a boiler which superheats the steam to approximately 500°C. Such an auxiliary boiler is represented in Fig. 4 surrounded by a dashed line to indicate that it is called to operate only when U_f<45%; in this case, the SH in the anode off-gas heat recovery line (section 19-20) is not used.

2.6. CO_2 and H_2 purification

Following earlier work on CO_2 purification, compression and liquefaction in MCFC plants with CO_2 capture [42–44] we assume here that, after being cooled down in the heat recovery section, the stream exiting the anode is treated by a cryogenic Gas Processing Unit (GPU) to separate the CO_2 from the H_2. Given the need to make hydrogen available at conditions typical of pipeline transmission (ca. 60 bar) and the low concentration of CO_2 at the GPU inlet (point #29) encountered when operating at low U_f, performance predictions for state-of-the-art GPU configurations must be adjusted. The cross-validation of the results presented in [45] with separation and compression work estimates reported in [46] has suggested the adoption of specific consumptions of 768 kJ $kgCO_2^{-1}$, 612 kJ $kgCO_2^{-1}$ and 512 kJ $kgCO_2^{-1}$ for U_f=45%, U_f=60% and U_f=75%, respectively.

The off-gas stream of the GPU section is processed in a PSA to produce high-purity H_2 (i.e., 99.999%). The PSA operating conditions are estimated according to a model based on the application of semi-empirical Langmuir adsorption isotherms for activated carbons (AC) and zeolite LiX [39]. The model sets the volume ratio in the adsorption columns between activated carbons and zeolite to 60% and, given the geometry of the columns and the adsorption/desorption cycle time, calculates the number of columns, the maximum operating pressure required to reach the target H_2 purity and the resulting H_2 recovery.

The PSA tail-gas rich in hydrogen and residual CO_2 is recycled to the catalytic oxidiser upstream of the MCFC cathode (point #38). By minimizing the impact on existing hydrogen production, this arrangement is particularly suitable for retrofit applications.

3. Results

3.1. Low fuel utilization factor operation

The operation at low fuel utilization brings about new challenges for the operation of the fuel cell. In the carbon capture framework considered here, the main trade-off is between the capability to transport enough CO_2 from the cathode to the anode, thus increasing the CO_2 capture rate and the operation at conditions that can warrant acceptable lifetime and limit performance degradation. These conditions translate into the requirement that the ΔT across the cathode and the anode is not too high to avoid harmful thermal stresses and detrimental temperature gradients.

To illustrate how low fuel utilization factors can affect the operating conditions of a MCFC aimed at capturing CO_2 while simultaneously producing electricity and hydrogen, Table 4 reports the basic operating parameters assumed/calculated under the following assumptions:

- The cell operates at the voltage and current density lying on the polarisation curve corresponding to the given fuel utilization factor, where the polarization curves are the same used in [26], which were calibrated against experimental data;
- 2.5% molar oxygen concentration at the cathode outlet is achieved by adjusting the air flow added to flue gases upstream of the cathode (as made possible by air stream #4 in Fig. 4);
- 1% molar CO_2 concentration at the cathode outlet is achieved by adjusting the mass flow rate of the pre-reformed stream entering the anode;
- 100% methane conversion in the pre-reforming layer and the anodic compartment. This is equivalent to assuming excess reforming kinetic capacity by the reforming catalyst, an assumption supported by [47]. This assumption likely breaks down at the very lowest fuel utilizations, leading to a small amount of CH_4 in the anode exhaust. However, modelling such minor contributions is beyond the scope of this paper and will not substantially impact the conclusions drawn;
- Current density is adjusted to achieve isothermal conditions (U_f=45%) or the maximum inlet-outlet ΔT (70°C) that can be withstood by the cell.

As the U_f is decreased, the heat required by the endothermic reforming of the fuel input is not completely provided by the exothermic electro-oxidation reactions and the voltage drop, leading potentially to a temperature drop across the cell. To compensate for this heat deficit, the cell potential must be decreased, thereby generating heat within the cell [48]. This "dissipative mode" to close the energy balance is obviously detrimental to electrical efficiency and voltage, but that reduced electrical efficiency is converted into increased hydrogen chemical energy. For the lowest U_f=45% considered in Table 4, the cell potential needed to make the cell isothermal is 0.654 V, which by our model is achieved with a current density of 2665 A m^{-2}. Notice that despite the inefficiencies arising from the large current densities, the "isothermal" case with U_f=45% in Table 4 exhibits the attractive features of internal cooling by chemical reactions rather than by convective heat transfer, potentially making the cell design more flexible, and small temperature gradients across the stack channels, whereby longer lifetime and lower degradation of the cell are expected.

For U_f =60% and even more for 75% the heat released by electro-oxidation reactions is greater than the heat used internally for steam reforming, yielding a temperature increase across the cell. The maximum ΔT of 70°C assumed here is reached for current densities of 2166 and 1014 A m^{-2} at U_f of 60% and 75%, respectively. The latter corresponds to a voltage of 0.787 V and very high electric efficiency thanks to low electrochemical losses (especially ohmic and activation overpotentials). On the other hand, the specific power per unit of active area is low, hence increasing the number of fuel cell stacks to be installed for the same power output.

Table 4
Operating conditions considered for a MCFC aimed at capturing CO_2 at different fuel utilization factors in carbon capture operation ($T_{an,inlet}$=600°C, $X_{CO2,Out}$=1%, $X_{O2,Out}$=2.5%).

	U_f = 45.0%	U_f = 60.0%	U_f = 75.0%
Cathode inlet	CO_2 = 13.4%; H_2O = 11.7%; N_2 = 65.7%; O_2 = 8.3%; Ar = 0.78%		
Anode inlet	CH_4 = 27.9%; CO_2 = 2.4%; H_2 = 7.0%; H_2O = 62.0%; N_2 = 0.6%		
Cathode inlet T	T_{cat} = 600°C	T_{cat} = 575°C	T_{cat}=575°C
Maximum ΔT_{cat}	ΔT_{cat} = 0°C (isothermal)	ΔT_{cat} = 70°C	ΔT_{cat} = 70°C
Outlet $T_{cat} = T_{an}$	600°C	645°C	645°C
Current density	2665 A/m^2	2166 A/m^2	1014 A/m^2
Cell voltage	0.654 V	0.686 V	0.787 V

Table 5
MCFC operating conditions within the retrofit plant layout.

U_f	%	45	60	75
U_{ox}	%	74.9	75.2	75.1
U_{CO2}	%	93.7	93.8	93.8
V_{cell}	V	0.654	0.686	0.787
I_{cell}	A/m^2	2665	2166	1014
T cathode inlet	°C	600	575	575
T cathode outlet	°C	600	645	645
ΔT cell cathode	°C	0.0	70	70
T_{in} pre-reforming layer	°C	500	475	450
T anode inlet	°C	600	600	600
T anode outlet	°C	600	645	645
ΔT cell anode	°C	100	170	195
x_{O2} inlet	%	8.13	8.23	8.19
x_{O2} outlet	%	2.50	2.50	2.50
x_{CO2} inlet	%	13.00	13.19	13.13
x_{CO2} outlet	%	1.00	1.00	1.00
MCFC Area	m^2	36,100	43,750	92,550

High electrical efficiencies and, at the same time, high power densities could be achieved by adopting multiple cells with cathodes connected in series (the flow exiting the first cathode enters the second cathode and so on, possibly with the addition of some air to provide oxygen) and anodes connected in parallel. By operating the cells with the same fuel utilization factor but different U_{CO2} and U_{Ox} one can adopt high current densities (whereby high power density) while limiting the maximum ΔT across the cells – an arrangement explored in [27] for CO_2 capture in the cement industry. The same arrangement could be replicated in the application to SMRs considered here to achieve a good compromise between MCFC electric efficiency and fuel cell stack count.

3.2. Overall performance

Table 5 summarizes the operating conditions of the MCFC when used in the scheme of Fig. 4 for U_f=45% (i.e., isothermal operation), U_f=60% and U_f=75%. In all cases, the U_{CO2} is kept the same, because the molar concentration of CO_2 at the cathode outlet is set to 1%. This allows for a fair comparison from a CO_2 emission standpoint, although current density and therefore power density, cell area per unit of energy and capital cost vary significantly. Table A2 gives thermodynamic conditions and composition at the points identified in Fig. 4 when operated at U_f = 45%.

Evaluation of the energy usage, efficiency, H_2 production, and emissions of the combined SMR+MCFC case is complicated because of the simultaneous production of power and hydrogen. We have adopted here a method in which credits (or debits) are given as appropriate for the co-product; the size of the credit (debit) is proportional to how the standalone system without CO_2 capture would have generated the H_2 or electricity. The credits can be applied by either beginning with the electrical efficiency and providing a credit for H_2 co-production or beginning with H_2 production efficiency and applying a credit for co-product power production. In the following formulas and in Table 8 we show both approaches, but focus our discussion on the latter comparison, as hydrogen production is the primary purpose of these systems. The energy flows and efficiencies without co-product credits are denoted by Q and η while with the co-product credit we refer to them as "adjusted" energy consumptions and efficiencies are denoted with a prime symbol, Q' and η'; the subscripts denote which stream and which adjustment (in parenthesis) is being made. For the reference systems, we use the SMR as described above (Table 2) and an NGCC with electrical efficiency of 58%.

$$\eta_{el,total} = \frac{\dot{W}_{el,total}}{\dot{Q}_{NG,total}} \tag{7}$$

$$\dot{Q}'_{NG,total(H_2)} = \dot{Q}_{NG,total} - \frac{\dot{Q}_{H_2,total}}{\eta^{ref}_{H_2}} \tag{8}$$

$$\eta'_{el,total} = \frac{\dot{W}_{el,total}}{\dot{Q}'_{NG,total(H_2)}} \tag{9}$$

$$\eta_{H_2,total} = \frac{\dot{Q}_{H_2,total}}{\dot{Q}_{NG,total}} \tag{10}$$

$$\dot{Q}'_{H_2,total(el)} = \dot{Q}_{NG,total} - \frac{W_{el,total}}{\eta^{ref}_{el}} \tag{11}$$

$$\eta'_{H_2,total} = \frac{\dot{Q}_{H_2,total}}{\dot{Q}'_{H_2,total(el)}} \tag{12}$$

$$\eta_{el+H_2,total} = \frac{\dot{W}_{el,total} + \dot{Q}_{H_2,total}}{\dot{Q}_{NG,total}} \tag{13}$$

We have also computed adjustments for just for the MCFC and CO_2 capture sub-system:

$$\eta_{el,MCFC} = \frac{\dot{W}_{el,MCFC}}{\dot{Q}_{NG,MCFC}} \tag{14}$$

$$\dot{Q}'_{NG,MCFC(H_2)} = \dot{Q}_{NG,MCFC} - \frac{\dot{Q}_{H_2,MCFC}}{\eta^{ref}_{H_2}} \tag{15}$$

$$\eta'_{el,MCFC} = \frac{\dot{W}_{el,MCFC}}{\dot{Q}'_{NG,MCFC(H_2)}} \tag{16}$$

$$\eta_{H_2,MCFC} = \frac{\dot{Q}_{H_2,MCFC}}{\dot{Q}_{NG,MCFC}} \tag{17}$$

$$\dot{Q}'_{NG,MCFC(el)} = \dot{Q}_{NG,MCFC} - \frac{\dot{W}_{el,MCFC}}{\eta^{ref}_{el}} \tag{18}$$

$$\eta'_{H_2,MCFC(el)} = \frac{\dot{Q}_{H_2,MCFC}}{\dot{Q}'_{NG,MCFC(el)}} \tag{19}$$

$$\eta_{el+H_2,MCFC} = \frac{\dot{W}_{el,MCFC} + \dot{Q}_{H_2,MCFC}}{\dot{Q}_{NG,MCFC}} \tag{20}$$

Table 6 compares the overall performances of the proposed system, at the three different levels of fuel utilization, with those of the reference FTR without CCS. Consider first the case at high fuel utilization of U_f = 75%. In this case, the fuel cells generate an additional 71.6 MW of electrical power, of which 19.1 MW is consumed by the H_2/CO_2 separation in the gas processing unit, leaving a net power production of 52.5 MW. This case also generates an additional 26.4 MW of H_2, after consumption by the catalytic combustor and losses in the GPU are accounted for. This H_2 production represents an increase of 9.1% over the base case, *while capturing 90% of the SMR's CO_2*.

Table 6
Overall performance summary of the reference FTR and SMR+MCFC system with CCS. All values are in MW on an LHV basis except for efficiencies, which are in percentages.

Parameter	Ref FTR	S+M+C, U_f=45%	S+M+C, U_f=60%	S+M+C, U_f=75%
NG inlet to SMR ($\dot{Q}_{NG,SMR}$)	380.3	380.3	380.3	380.3
NG inlet to MCFC ($\dot{Q}_{NG,MCFC}$)		222.5	164.3	130.1
Total NG inlet ($\dot{Q}_{NG,tot}$)		602.8	544.5	510.3
H_2 from SMR ($\dot{Q}_{H_2,SMR}$)	291.3	291.3	291.3	291.3
Gross H_2 production by MCFC ($\dot{Q}_{H_2,MCFC,gr}$)		145.0	77.9	38.7
H_2 consumed by MCFC catalytic combustor		-16.6	-10.3	-10.8
H_2 consumed by SH catalytic combustor		-13.5	n/a	n/a
H_2 lost in GPU		-5.5	-2.9	-1.5
Net H_2 production by MCFC ($\dot{Q}_{H_2,MCFC,net}$)		109.4	64.7	26.4
Net H_2 production from SMR and MCFC ($\dot{Q}_{H_2,tot}$)		400.8	356.0	317.7
Increase in H_2 production		37.6%	22.2%	9.1%
Steam cycle gross power	6.1	6.1	6.1	6.1
SMR auxiliary power consumption	-6.1	-6.1	-6.1	-6.1
Fuel cell gross power ($\dot{W}_{el,MCFC}$)		61.0	63.1	71.6
MCFC/GPU auxiliary power consumption		-35.2	-24.9	-19.1
Net power production ($\dot{W}_{el}$)	0.0	25.9	38.1	52.5
Total net electric efficiency ($\eta_{el,total}$)	0%	4.3%	7.0%	10.3%
Adjusted total NG consumption ($\dot{Q}'_{NG,total(H_2)}$)		79.6	80.1	95.8
Adjusted total net electrical efficiency ($\eta'_{el,total}$)	0%	32.6%	47.6%	54.8%
MCFC net electric efficiency ($\eta_{el,MCFC}$)		11.7%	23.2%	40.4%
Adjusted MCFC NG consumption ($\dot{Q}'_{NG,total(H_2)}$)		79.6	80.1	95.8
Adjusted MCFC net electric efficiency ($\eta'_{el,MCFC}$)		32.6%	47.6%	54.8%
Total H_2 efficiency ($\eta_{H_2,total}$)	76.6%	66.5%	65.3%	62.2%
Adjusted total NG consumption ($\dot{Q}'_{NG,total(el)}$)		558.1	478.8	419.7
Adjusted total H_2 efficiency ($\eta'_{H_2,total}$)	76.6%	71.8%	74.3%	75.7%
MCFC net H_2 efficiency ($\eta_{H_2,MCFC}$)		49.2%	39.2%	20.2%
Adjusted MCFC NG consumption ($\dot{Q}'_{NG,MCFC(el)}$)		177.8	98.5	39.5
Adjusted MCFC Net H_2 efficiency ($\eta'_{H_2,MCFC}$)		61.6%	65.4%	66.4%
Total first law net efficiency ($\eta_{el+H_2,total}$)	76.6%	70.8%	72.3%	72.5%
MCFC first law net efficiency ($\eta_{el+H_2,MCFC}$)		60.8%	62.5%	60.6%

The hydrogen production efficiency of the U_f = 75% case is calculated in Table 6 as 62.3%, which is to be compared with an efficiency of 76.6% of the reference case without capture. However, this efficiency disregards the co-production of electricity. The combined efficiency, $\eta_{el+H_2,total}$, is 72.6%, which is comparable to the 76.6% value of the reference case. However, in the MCFC scenario, the products are largely H_2, but – on an energy basis – are 14% electricity as well. Adjusting the hydrogen efficiency to account for the power production, using a 58% thermally efficient NGCC, moves the hydrogen efficiency to 75.6%, or just a slight reduction in hydrogen production efficiency. The reduction is so small because the MCFCs are efficient devices for power production, but even more efficient at the simultaneous production of power and hydrogen and CO_2 capture. In contrast, the use of an amine unit on the combustion flue gas of an SMR decreases the hydrogen production efficiency to 69.2%, as estimated by Collodi [9], or 64.3% as reported by Herraiz [17].

As the fuel utilization is decreased, hydrogen generation is increased with corresponding decreased electrical output. The increase of H_2 production capacity made possible by the carbonate fuel cells ranges from 9% (U_f=75%) to 37.6% (U_f=45%). In all cases, the retrofitted SMR can export low-carbon electricity to the grid or to a nearby industrial consumer. The largest auxiliary power load of the retrofitted system is the GPU and CO_2 compression, accounting for 18-40% of total auxiliary load consumption. The increase in natural gas consumption ranges from 34.2% with U_f=75% to 58.5% with U_f=45%, with an incremental H_2 efficiency ranging from 20.3% (U_f=75%) to 49.2% (U_f=45%). The adjusted H_2 production efficiency decreases slightly to 71.8%, reflecting the exchange of electricity for hydrogen and the increased parasitic electricity demand to compress and separate the H_2 from the CO_2.

3.3. Avoided emissions

Table 7 reports the amount of CO_2 emitted or captured per unit mass and per unit of chemical energy (LHV) of hydrogen; we denote the latter as e_{CO_2,H_2} with the units of kg CO_2 GJ^{-1} of H_2. As shown in the table, the specific direct CO_2 emissions of the proposed system are 90% to 95% lower than those of the reference SMR plant, for two reasons. First, the

Table 7
Specific direct CO_2 emissions and CO_2 capture per unit mass and per unit LHV of hydrogen produced at different fuel utilization factors.

Parameter	Unit	Ref FTR	S+M+C, U_f=45%	S+M+C, U_f=60%	S+M+C, U_f=75%
CO_2 emitted	kg CO_2 kg H_2^{-1}	8.66	0.44	0.48	0.54
CO_2 emitted	kg CO_2 GJ H_2^{-1}	72.2	3.7	4.0	4.5
CO_2 captured	kg CO_2 kg H_2^{-1}		9.5	9.7	10.1
CO_2 captured	kg CO_2 GJ H_2^{-1}		79.5	80.6	84.4
CO_2 capture ratio (CCR)	%	0%	95.6%	95.3%	95.0%

MCFCs capture the CO_2 from the SMR furnace, reducing the emissions. Second, the MCFCs also make additional H_2, as discussed above. This hydrogen is essentially CO_2-free because any CO_2 generated in the anode from the natural gas feed to the anode is nearly 100% captured by the system (only a small amount of CO_2 returns to the system via the oxidiser before the cathode). This illustrates the utility of the MCFCs: they generate CO_2-free power, CO_2-free hydrogen, both while capturing CO_2 from the SMR furnace. It should be noted that the emissions factors shown in Table 7 ascribe all the CO_2 emissions to the H_2, and none to the power. Stated differently, there is no credit given to the CO_2 emissions shown in Table 7 for the emissions avoided by the power production.

Table 7 also shows the CO_2 Capture Ratio, or CCR, which for all three MCFC cases is above 95%. In general, the CO_2 capture community targets 90% capture. We did not target a certain CO_2 capture rate in this work, but instead set the CO_2 concentration at the cathode outlet at 1% to avoid the complication of the hydroxide chemistry as reported by Rosen [23]. As shown in Table A2, the cathode inlet has a CO_2 concentration of about 13% (stream 8), so that an exit concentration of 1% (stream 9) means a CO_2 capture rate from the SMR furnace of 92%. The actual CCR is higher than this because any carbon fed to the anode inlet is captured with nearly 100% efficiency; only a small amount of carbon is recycled to the cathode oxidiser. Thus, the overall CO_2 capture rate is higher than the direct SMR exhaust capture rate. An even higher capture rate than 95% could be achieved if the cathode exit CO_2 concentration is reduced further, which is the subject of active research. It is very possible that by the time a facility such as this could be constructed, the performance of the fuel cells will be improved such that an exit concentration of 0.5%, or even less, is feasible, implying a CCR of 97% or even 98%. When combined with the excellent thermodynamic efficiency discussed previously, the combination of such a high CCR with such a small energy debit is unprecedented in CO_2 capture technologies.

Fig. 5 depicts the carbon flow diagram of the plant operating at U_f = 45%. Most of the carbon in the flue gases coming from the SMR is diverted from the cell cathode to the cell anode, from which it goes to the GPU and then to storage. A small fraction is "recycled" to the catalytic oxidiser, establishing the internal loop associated to the use of the PSA tail gas as fuel for the catalytic combustor placed upstream of the cathode inlet.

The proper evaluation of the potential for the reduction of CO_2 emissions of the proposed system must account for the emissions displaced by the production of additional (with respect to the reference SMR) hydrogen and electricity. In fact, the hydrogen and electricity generated by the MCFC system substitute hydrogen and electricity that would be generated with significantly higher CO_2 emissions by reference facilities without CO_2 capture. As was done with the efficiency calculations, above, the avoided emissions have been adjusted by considering a reference system comprising the "reference SMR" described in Section 2.3 and a state-of-the-art Natural Gas Combined Cycle (NGCC) with electric efficiency 58% and specific CO_2 emission of 342.6 kg CO_2 MWh_{el}^{-1} or 95.2 kg CO_2 GJ_{el}^{-1} (see Fig. 6).

Table 8 reports the overall picture for the CO_2 emissions. The primary energy fed to the SMR+MCFC system with CO_2 capture is Q^P_{S+M+C}, whereas the equivalent primary energy of the reference case (Q^P_{Ref}) is given by the sum in Eq. (21): (i) $\dot{Q}_{NG,ref}$, reflecting the natural gas consumption by the reference FTR, producing 291.3 MW_{LHV} of hydrogen and nearly zero electric power (37 kW_{el}); (ii) $\dot{Q}_{H_2,MCFC}/\eta^{ref}_{H_2}$, accounting for the fuel consumption of an additional FTR producing the same amount of net hydrogen generated by the MCFC system, with the same performance of the reference FTR; (iii) $\dot{W}_{el,S+M+C}/\eta^{ref}_{el}$, accounting for the fuel consumption of the reference NGCC producing the same net electric power generated by the SMR+MCFC system. Equivalent CO_2 emissions for the reference case ($\dot{E}_{CO2,\ Ref}$) are calculated following the same logic as for the fuel consumption (Eq. (22)).

$$\dot{Q}^p_{Ref} = \dot{Q}_{NG,ref} + \frac{\dot{Q}_{H_2,MCFC}}{\eta^{ref}_{H_2}} + \frac{\dot{W}_{el,S+M+C}}{\eta^{ref}_{el}} \quad (21)$$

$$\dot{E}_{CO_2,\ Ref} = \dot{Q}_{H_2,S+M+C} \cdot e^{ref}_{CO_2,H_2} + \dot{W}_{el,S+M+C} \cdot e^{ref}_{CO_2,\ el} \quad (22)$$

The result of these calculations is the amount of CO_2 emissions that are *avoided* per unit of H_2 (the bottom two rows of Table 8), which vary from 74.6 to 83.4 kg CO_2 GJ^{-1} H_2 for the different cases. "Avoided" emissions are to be thought of as "not emitted for equivalent H_2 production". This is a remarkable result, given that the emissions of the unabated SMR (Table 2) are only 72.2 kg CO_2 GJ^{-1} H_2 and the CCR is around 95% for each case. The integrated system using carbonate fuel cells is *avoiding* more CO_2 than was created in the first place, and avoiding more CO_2 than is fed to the system in the form of CH_4, due to the additional power generation by the MCFCs, which prevents an NGCC facility from emitting CO_2. This result is even more remarkable after noting that there is a considerable power debit for the CO_2 capture cases to compress the anode effluent and separate the H_2 and CO_2. This metric shows the extremely high efficacy of the carbonate fuel cells to simultaneously capture CO_2, generate H_2, and generate power.

A final metric to be considered for this system is the Specific Primary Energy Consumption per $CO_{2,eq}$ Avoided (SPECCA), as first introduced by Campanari et al. 2010 [25]:

$$SPECCA = \frac{\dot{Q}^p_{CCS} - \dot{Q}^p_{Ref}}{\dot{E}_{CO2,Ref} - \dot{E}_{CO_2,S+M+C}} = \frac{\dot{Q}^p_{S+M+C} - \dot{Q}^p_{Ref} - \frac{\dot{Q}_{H_2,MCFC}}{\eta^{ref}_{H_2}} - \frac{\dot{W}_{el,MCFC}}{\eta^{ref}_{el}}}{\dot{Q}_{H_2,S+M+C} \cdot e^{ref}_{CO_2,H_2} + \dot{W}_{el,S+M+C} \cdot e^{ref}_{CO_2,\ el} - \dot{E}_{CO_2,S+M+C}} \quad (23)$$

SPECCA represents the additional energy required by the system to avoid CO_2 emissions compared to a reference system without CCS. For reference, the amine system described by Collodi [9] achieves a comparable CCR of 90% (and 89% avoided) and has a SPECCA of 1.95 MJ kg^{-1}. Our simulations show a SPECCA of 1.17, 0.52, and 0.20 MJ kg^{-1} for fuel utilizations of 45%, 60%, and 75%, respectively. These are quite low relative to the amine system, and have a higher CCR of at least 95%, and avoided CO_2 ratios of more than 100%. Collodi also evaluated the option of capturing only the process CO_2, that is, the CO_2 in the syngas stream. The four scenarios they studied have SPECCA values that range from 1.06 to -0.07 MJ kg^{-1} but have capture ratios limited to only 53 to 67%. The MCFC systems presented here show superior performance in all respects – higher capture rate, higher avoided rate, and lower energy consumption.

Fig. 7 summarizes these results for the three cases considered here and illustrates the flexibility that the system may have for the SMR

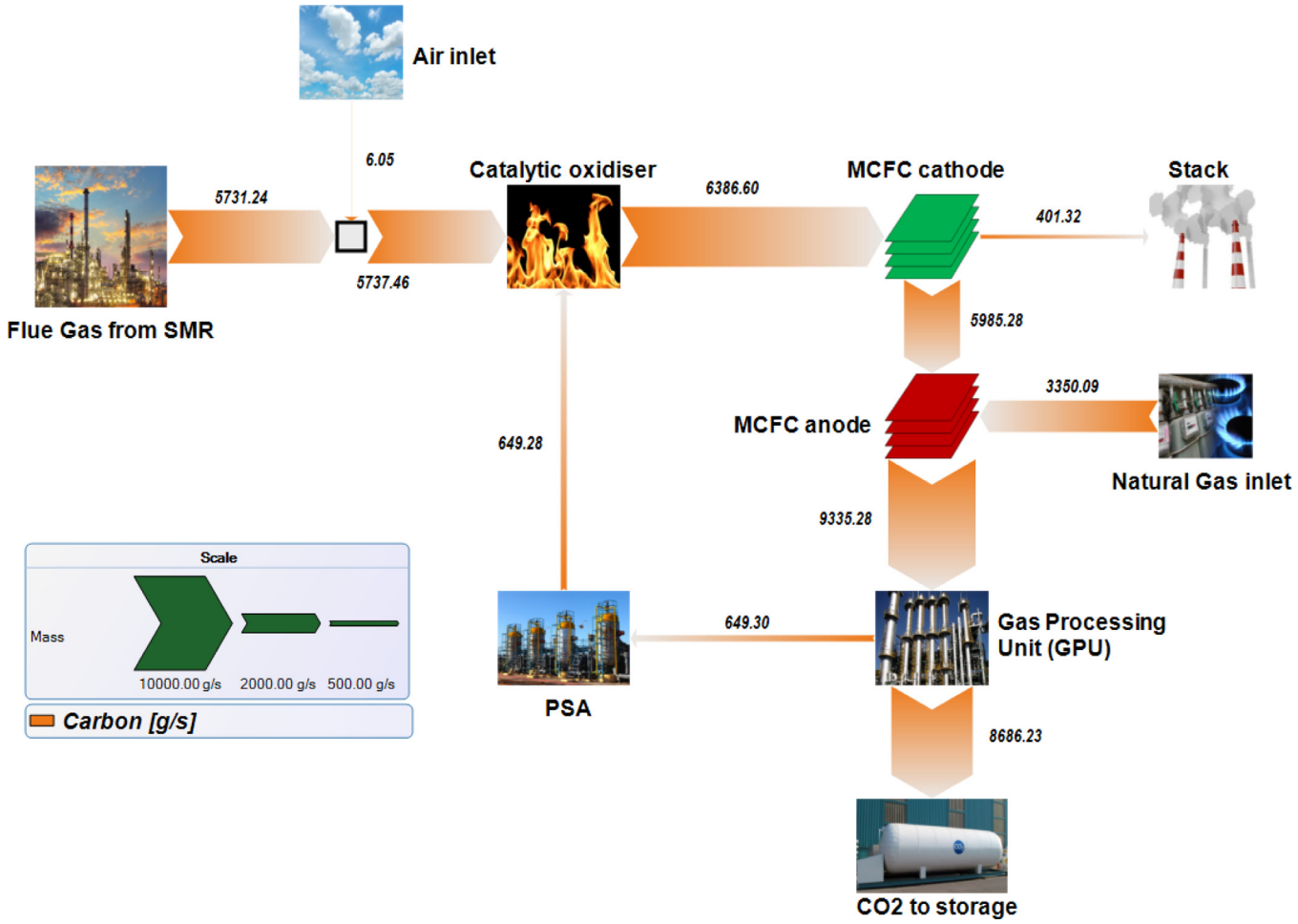

Fig. 5. Carbon flow diagram for the SMR-MCFC retrofit system when operated at U_f = 45%.

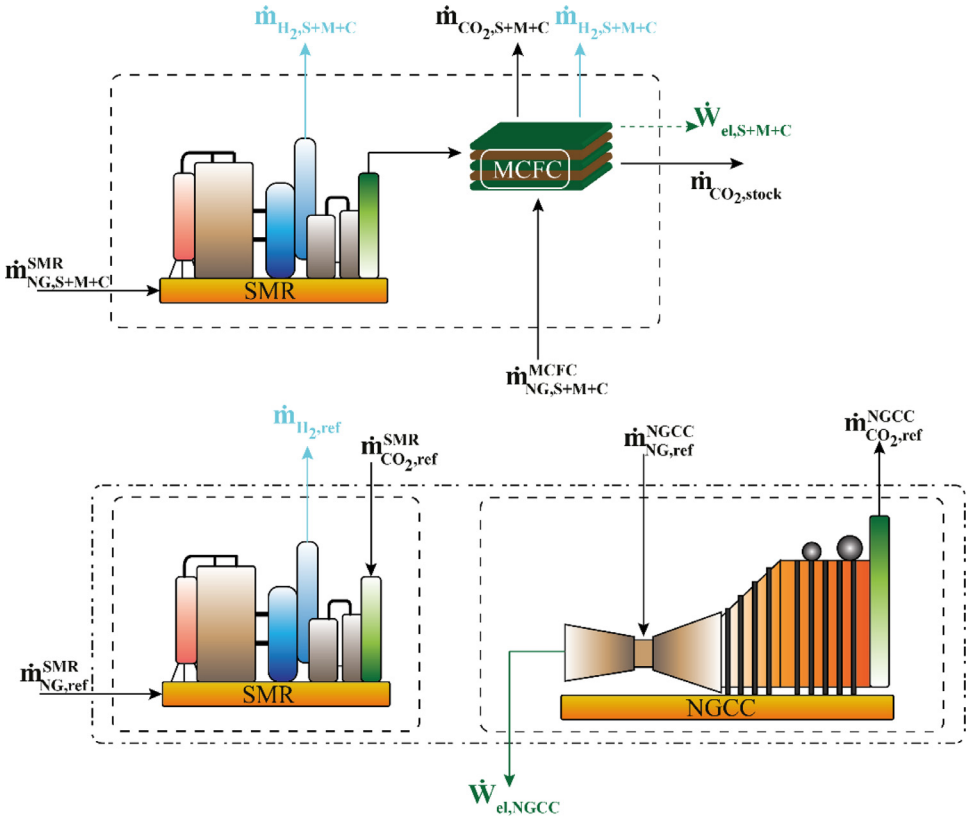

Fig. 6. Systems considered to assess the energy and CO_2 emission performance of the retrofit proposed here. The figure at the top represents the S+M+C system with carbon capture. The figure at the bottom represents the reference FTR described in Section 2.3, together with the reference NGCC.

Table 8
Avoided emissions of the SMR+MCFC system operated at different fuel utilization factors. Avoided emissions are those that would be generated by the reference FTR described in Section 2.3 and a reference NGCC for a comparable production of H_2 and electricity.

#	Parameter	Unit	S+M+C, U_f =45%	S+M+C, U_f =60%	S+M+C, U_f =75%
$e^{ref}_{CO_2,\ el}$	Specific CO_2 emissions of the reference electricity producer	kg $_{CO2}$/MWh$_{el}$ (kg $_{CO2}$/GJ$_{el}$)		— 342.6 (95.2) —	
$e^{ref}_{CO_2,\ H_2}$	Specific CO_2 emissions of the reference hydrogen producer	kg $_{CO2}$/GJ$_{H2}$		— 72.2 —	
$\dot{E}_{CO_2,S+M+C}$ ("A")	CO_2 emissions of each MCFC case	kg CO_2/s	1.47	1.42	1.42
$\frac{\dot{Q}_{H_2,S+M+C}}{e^{ref}_{CO_2,H_2}}$ ("B")	CO_2 emissions of the reference SMR for the H_2 produced by the MCFC case	kg CO_2/s	28.9	25.7	22.9
$\frac{\dot{W}_{el_{MCFC+SMR}}}{e^{ref}_{CO_2,\ el}}$ ("C")	CO_2 emissions of the reference NGCC for the net power produced by the MCFC cases	kg CO_2/s	2.47	3.63	5.00
B + C − A	CO_2 avoided, or not emitted, by the MCFC case relative to the equivalent reference case	kg CO_2/s	29.9	27.9	26.5
$\frac{B+C-A}{\dot{Q}_{H_2,S+M+C}}$	CO_2 avoided per unit of H_2 produced (energy)	kg CO_2/GJ H_2	74.6	78.4	83.4
	CO_2 avoided per unit of H_2 produced (mass)	kg CO_2/kg H_2	9.0	9.4	10.0
SPECCA	Specific Primary Energy Consumption for CO_2 Avoided	MJ/kg CO_2	1.17	0.52	0.20

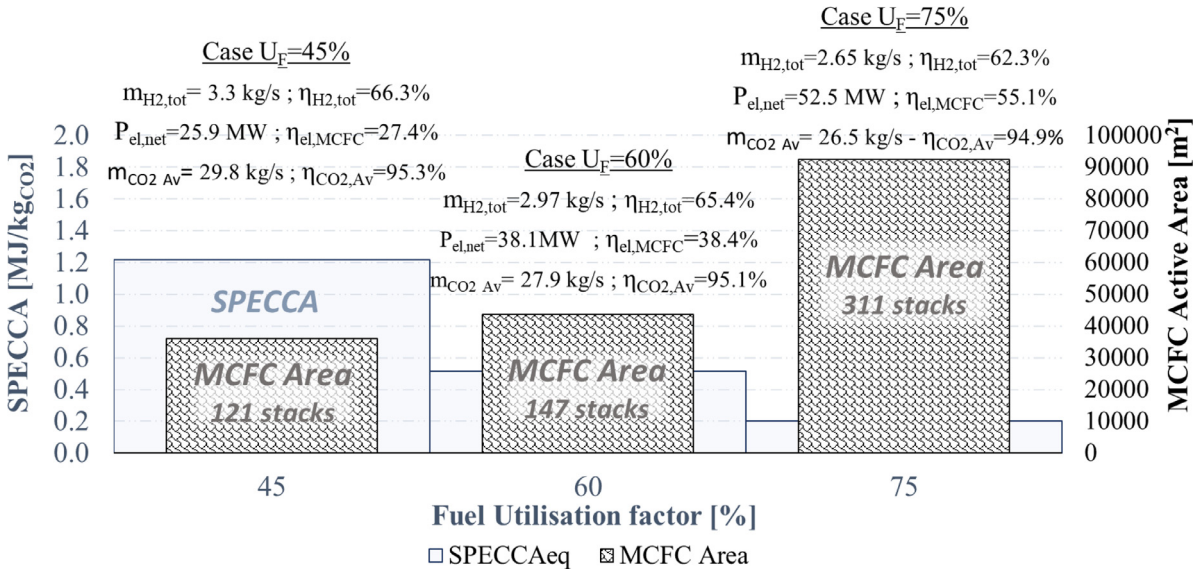

Fig. 7. SPECCA and MCFC active area vs fuel utilization factor U_f.

owner. At low U_f, more H_2 is produced, by fewer fuel cells, but at a higher energy penalty relative to the cases at high U_f. This means that the system owner can choose between the different scenarios to employ based on market conditions, which can vary from location to location. It should be noted, though, that once the system is installed and operational, it will not be feasible to swing from the highest U_f to the lowest U_f; the internal structure of the fuel cell stacks will be different because of the different temperature regimes. There will be some allowable variation around the design point, but not a change of 30%.

The lower U_f demands a higher current density (due to the operating assumptions discussed in Section 3.1) and a higher electrochemical loss inside the cell to generate the heat required for reforming. This reduces the cell voltage (by 20% when U_f goes from 75% to 45%) as well as the gross/net electric power produced by the MCFC. The net electrical efficiency gap with respect to the reference NGCC increases, and so does the SPECCA. On the other hand, the operation at high current density allows reducing the MCFC area to less than half, representing a significant capital savings.

Table 8 and Fig. 8 show how the SMR+ MCFC with CO_2 capture benefits from the synergy among the three basic "services" that it provides: production of electricity, production of hydrogen and carbon capture. If compared to the reference FTR plant emitting 663 kton y^{-1}, all three SMR+MCFC configurations generate a higher amount of CO_2 (up to +40%) due to the additional NG converted in the fuel cell section. However, the CO_2 emitted to atmosphere by the SMR+MCFC with capture is only about 45 kt$_{CO2}$ y^{-1} (4 - 5% of the CO_2 generated) and the displacement of hydrogen production from reference FTRs and of electricity production for reference NGCCs allows the system to avoid 880-1000 kton y^{-1} of CO_2 emissions.

The fuel utilization factor has a negligible effect on the amount of CO_2 emitted, because in all cases the concentration of CO_2 in the cathode exhausts released to atmosphere is just 1%. A fuel utilization of 45% gives a relatively large difference between CO_2 captured and CO_2 avoided, because of the limited amount of carbon-free net electric power output: 26 MW$_e$, corresponding to 77 kton y^{-1} of CO_2 avoided. At higher utilization factors carbon-free net power output increases ow-

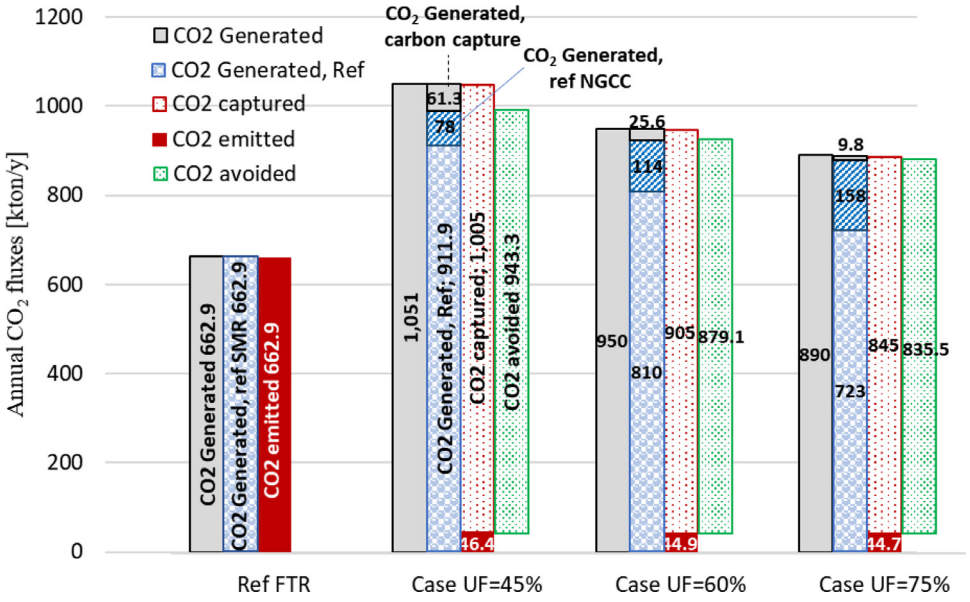

Fig. 8. CO_2 generated, emitted, captured, and avoided for the selected cases (annual basis). The "CO_2 generated" figure corresponds to the totality of equivalent CO_2 entering the system with air and fuel streams for both the reference and the S+M+C systems. The "CO_2 Generated, carbon capture" highlights the additional CO_2 generated from the S+M+C plant due to the higher fuel input. The "CO_2 emitted" figure accounts for the CO_2 effectively vented at the stack. The "CO_2 avoided" figure considers the CO_2 displaced in the reference systems due to the production of low-carbon products. The "CO_2 captured" figure refers to the CO_2 captured by the S+M+C plant.

ing to the higher MCFC efficiency and to lower auxiliary consumption; with U_f=75% the net electric power of 52.5 MW_e generates 155 kton/y of avoided emissions and total CO_2 avoided (836 kton y^{-1}) approaches CO_2 captured (845 kton y^{-1}).

Besides giving the largest avoided emissions (941 kton y^{-1}) U_f=45% requires a MCFC area much below the one required by the other cases. Adding the advantages that nearly iso-thermal operation can produce on cell life makes the design at low fuel utilization factors extremely attractive for the retrofit proposed here.

4. Conclusions

The retrofit of SMR plants with MCFCs geared toward CO_2 capture can give a tenfold reduction of specific direct CO_2 emissions, together with a significant increase of hydrogen production capacity and the export of substantial amounts of electricity. These synergistic effects make SMR+MCFC systems particularly attractive for creating "blue" hydrogen from SMRs, when coupled with appropriate CO_2 sequestration technologies. We have modelled here the retrofit case of adding the MCFCs to an existing SMR, with minimal integration between them. If a grassroots system were considered, the results may be even better still, given the opportunity to integrate the H_2 purification in the SMR plant with the H_2/CO_2 separation required for the anode product.

Unlike conventional fuel cell applications for which the sole goal is the production of electricity, the retrofit of SMR plants arouses interest in operating the fuel cell at low fuel utilization factors to boost the production of hydrogen at the expense of the production of power. To understand the trade-off between the production of hydrogen and the production of power, as well as its impact on the operating conditions of the cell, we've modelled the MCFC system with CO_2 capture for three values of the fuel utilization factor U_f ranging from 45% to 75%. U_f = 45% allows operating the fuel cell close to iso-thermal conditions, where the heat generated by exothermic electro-oxidation reactions approximately balances the heat required by endothermic reforming reactions. At U_f=75%, the value typically adopted for the production of power only, exothermic reactions prevail and current density must be limited to avoid undue thermal stresses and unsafe ΔT across the stack. The much higher current densities that can be adopted at low U_f can give substantial reduction of MCFC area and therefore their capital cost.

The MCFC system proposed here would allow an incremental production of hydrogen between 20 and 50% of the production of the SMR being retrofitted, at the expense of an increase of natural gas consumption between 34 and 58%. The overall LHV efficiency of the production of decarbonized hydrogen ranges 62-66%, which compares with the 77% efficiency of a conventional SMR without CCS. The first law efficiency of the co-production of decarbonized hydrogen and electricity ranges 71-73%.

About 95% of the CO_2 generated within the retrofitted SMR+MCFC plant are captured on site. After accounting for the emissions displaced by the production of nearly carbon-free hydrogen and electricity, the overall emission balance for the retrofit of the reference FTR with hydrogen production capacity 291.3 MW_{LHV} gives negative CO_2 emissions ranging from 835 to 941 kton/y depending on the MCFC fuel utilization factor.

Declaration of Competing Interest

Timothy A. Barckholtz is an employee of ExxonMobil Research and Engineering and holds many patents and patent applications in this area. ExxonMobil and its research partner FuelCell Energy are working on the development and commercialization of this technology.

CRediT authorship contribution statement

Stefano Consonni: Conceptualization, Funding acquisition, Project administration, Supervision, Writing – review & editing. **Luca Mastropasqua:** Conceptualization, Investigation, Formal analysis, Software, Visualization, Writing – original draft, Writing – review & editing. **Maurizio Spinelli:** Visualization, Methodology, Writing – review & editing. **Timothy A. Barckholtz:** Data curation, Resources, Supervision, Writing – review & editing. **Stefano Campanari:** Supervision, Writing – review & editing.

Acknowledgment

The authors gratefully acknowledge Dr. Eric Larson and Dr. Tom Kreutz for the constructive discussions and the original thoughts originated during the visit of Prof. Consonni and Dr. Mastropasqua at the Andlinger Centre for Energy and Environment of Princeton University within the framework of the Princeton E-ffiliates Partnership, in the Spring Semester of 2018.

Appendix

Tables A1 and A2

Table A1
Thermodynamic conditions of the flows numbered in Fig. 1 for the reference CHP plant without CCS.

	T °C	p bar	G kg s^{-1}	Ar v/v %	CH_4	CO	CO_2	C_2H_6	C_3H_8	C_4H_{10}	H_2	H_2O	N_2	O_2	H_2O(L)
1	20	1.01	0.500	0.92	0.0	0.0	0.03	0.0	0.0	0.0	0.0	1.03	77.28	20.73	0.0
2	30.1	1.11	0.500	0.92	0.0	0.0	0.03	0.0	0.0	0.0	0.0	1.03	77.28	20.73	0.0
3	579.9	1.1	0.696	0.67	0.0	0.0	14.28	0.0	0.0	0.0	0.0	15.76	56.47	12.82	0.0
4	624.5	1.08	0.548	0.80	0.0	0.0	4.65	0.0	0.0	0.0	0.0	18.65	66.86	9.05	0.0
5	435.9	1.06	0.548	0.80	0.0	0.0	4.65	0.0	0.0	0.0	0.0	18.65	66.86	9.05	0.0
6	60	1.04	0.548	0.80	0.0	0.0	4.65	0.0	0.0	0.0	0.0	18.65	66.86	9.05	0.0
7	50	3.01	1.887	-	-	-	-	-	-	-	-	-	-	-	-
8	80	2.95	1.887	-	-	-	-	-	-	-	-	-	-	-	-
9	15	1.14	0.015	0.0	89.01	0.0	2.00	7.00	1.10	0.0	0.0	0.0	0.89	0.0	0.0
10	450	1.11	0.015	0.0	89.01	0.0	2.00	7.00	1.10	0.0	0.0	0.0	0.89	0.0	0.0
11	15	1.14	0.033	-	-	-	-	-	-	-	-	-	-	-	-
12	450	1.11	0.033	-	-	-	-	-	-	-	-	-	-	-	-
13	449.7	1.11	0.048	0.0	28.47	0.0	0.64	2.24	0.35	0.0	0.0	68.01	0.29	0.0	0.0
14	624.5	1.03	0.196	0.0	0.0	5.03	43.64	0.0	0.0	0.0	10.84	40.37	0.11	0.0	0.0

Table A2
Thermodynamic conditions and chemical molar composition of the main point of the proposed layout operated at U_f = 45%.

	T °C	p bar	ṁ kg s^{-1}	Ar % vol	CH_4	CO	CO_2	C2+	H_2	H_2O	N_2	O_2	H_2O
1	154.9	1.0	68.76	0.70	-	-	20.56	-	-	18.28	59.46	1.00	-
2	173.0	1.2	68.76	0.70	-	-	20.56	-	-	18.28	59.46	1.00	-
3	173.0	1.2	68.76	0.70	-	-	20.56	-	-	18.28	59.46	1.00	-
4	30.2	1.2	48.48	0.92	-	-	0.03	-	-	1.03	77.28	20.73	-
5	117.0	1.2	117.25	0.79	-	-	11.94	-	-	11.04	66.94	9.28	-
6	250.0	1.1	117.25	0.79	-	-	11.94	-	-	11.04	66.94	9.28	-
7	473.9	1.1	117.25	0.79	-	-	11.94	-	-	11.04	66.94	9.28	-
8	600.1	1.1	119.76	0.78	-	-	13.01	-	-	12.48	65.60	8.14	-
9	599.9	1.1	89.83	0.95	-	-	1.00	-	-	15.27	80.28	2.50	-
10	320.0	1.0	89.83	0.95	-	-	1.00	-	-	15.27	80.28	2.50	-
11	153.5	1.0	89.83	0.95	-	-	1.00	-	-	15.27	80.28	2.50	-
12	153.5	1.0	89.83	0.95	-	-	1.00	-	-	15.27	80.28	2.50	-
13	15.0	1.4	4.62	-	95.00	-	-	3.00	-	-	2.00	-	-
14	280.0	1.3	4.62	-	95.00	-	-	3.00	-	-	2.00	-	-
15	450.0	1.3	15.68	-	29.49	-	-	0.93	-	68.96	0.62	-	-
16	360.9	1.3	15.68	-	27.47	0.01	2.37	-	8.63	60.92	0.59	-	-
17	500.0	1.3	15.68	-	27.47	0.01	2.37	-	8.63	60.92	0.59	-	-
18	600.0	1.2	45.61	-	-	7.81	32.14	-	23.49	36.28	0.28	-	-
19	529.0	1.2	45.61	-	-	7.81	32.14	-	23.49	36.28	0.28	-	-
20	529.0	1.2	45.61	-	-	7.81	32.14	-	23.49	36.28	0.28	-	-
21	340.0	1.2	45.61	-	-	7.81	32.14	-	23.49	36.28	0.28	-	-
22	386.9	1.2	45.61	-	-	3.12	36.82	-	28.18	31.60	0.28	-	-
23	376.4	1.1	45.61	-	-	3.12	36.82	-	28.18	31.60	0.28	-	-
24	334.5	1.1	45.61	-	-	3.12	36.82	-	28.18	31.60	0.28	-	-
25	186.5	1.1	45.61	-	-	3.12	36.82	-	28.18	31.60	0.28	-	-
26	180.0	1.1	45.61	-	-	3.12	36.82	-	28.18	31.60	0.28	-	-
27	147.6	1.0	45.61	-	-	0.52	39.42	-	30.78	29.00	0.28	-	-
28	45.0	1.0	45.61	-	-	0.52	39.42	-	30.78	7.41	0.28	-	21.59
29	45.0	1.0	38.04	-	-	0.67	50.27	-	39.25	9.45	0.36	-	-
30	45.0	2.3	3.54	-	-	1.38	7.13	-	90.74	-	0.75	-	-
31	112.0	8.6	3.54	-	-	1.38	7.13	-	90.74	-	0.75	-	-
32	45.0	8.5	3.54	-	-	1.38	7.13	-	90.74	-	0.75	-	-
33	45.0	8.5	1.04	-	-	-	-	-	> 99.9	-	-	-	-
34	50.0	60.0	0.91	-	-	-	-	-	> 99.9	-	-	-	-
35	45.0	8.5	0.01	-	-	-	-	-	> 99.9	-	-	-	-
36	45.0	8.5	2.50	-	-	7.20	37.19	-	51.71	-	3.90	-	-
37	45.0	8.5	2.51	-	-	6.89	35.59	-	53.79	-	3.74	-	-
38	230.0	8.3	2.51	-	-	6.89	35.59	-	53.79	-	3.74	-	-
39	45.0	8.5	0.11	-	-	-	-	-	> 99.9	-	-	-	-
40	15.0	1.0	38.93	0.92	-	-	0.03	-	-	1.03	77.28	20.73	-
41	400.0	1.1	38.93	0.92	-	-	0.03	-	-	1.03	77.28	20.73	-
42	463.3	1.0	39.04	0.90	-	-	0.03	-	-	5.05	75.72	18.30	-
43	100.0	1.0	39.04	0.90	-	-	0.03	-	-	5.05	75.72	18.30	-
44	15.0	1.5	11.07	-	-	-	-	-	-	-	-	-	100.0
45	107.0	1.5	6.33	-	-	-	-	-	-	-	-	-	100.0
46	107.0	1.5	4.73	-	-	-	-	-	-	-	-	-	100.0
47	113.0	1.5	4.73	-	-	-	-	-	-	100.0	-	-	-
48	113.0	1.5	6.33	-	-	-	-	-	-	100.0	-	-	-
49	113.0	1.5	11.07	-	-	-	-	-	-	100.0	-	-	-
50	113.0	1.5	11.07	-	-	-	-	-	-	100.0	-	-	-
51	559.8	1.4	11.07	-	-	-	-	-	-	100.0	-	-	-
52	45.0	1.0	31.90	-	-	0.19	96.68	-	3.03	-	0.10	-	-

References

[1] International Energy Agency (IEA), World energy outlook 2016, (2016) 684. www.iea.org/t&c/.

[2] H. Thomas, F. Armstrong, N. Brandon, B. David, A. Barron, J. Durrant, A. Guwy, A. Kucernak, M. Lewis, J. Maddy, I. Metcalfe, A. Porch, Options for producing low-carbon hydrogen at scale, 2018.

[3] Abe JO, Popoola API, Ajenifuja E, Popoola OM. Hydrogen energy, economy and storage: review and recommendation. Int J Hydrogen Energy 2019;44:15072–86. doi:10.1016/j.ijhydene.2019.04.068.

[4] Voldsund M, Jordal K, Anantharaman R. Hydrogen production with CO_2 capture. Int J Hydrogen Energy 2016;41:4969–92. doi:10.1016/j.ijhydene.2016.01.009.

[5] Vega F, Baena-Moreno FM, Gallego Fernández LM, Portillo E, Navarrete B, Zhang Z. Current status of CO_2 chemical absorption research applied to CCS: towards full deployment at industrial scale. Appl Energy 2020;260:114313. doi:10.1016/j.apenergy.2019.114313.

[6] Nikolaidis P, Poullikkas A. A comparative overview of hydrogen production processes. Renew Sustain Energy Rev 2017;67:597–611. doi:10.1016/j.rser.2016.09.044.

[7] Parkinson B, Tabatabaei M, Upham DC, Ballinger B, Greig C, Smart S, McFarland E. Hydrogen production using methane: techno-economics of decarbonizing fuels and chemicals. Int J Hydrogen Energy 2018;43:2540–55. doi:10.1016/j.ijhydene.2017.12.081.

[8] Khojasteh Salkuyeh Y, Saville BA, MacLean HL. Techno-economic analysis and life cycle assessment of hydrogen production from natural gas using current and emerging technologies. Int J Hydrogen Energy 2017;42:18894–909. doi:10.1016/j.ijhydene.2017.05.219.

[9] Collodi G, Azzaro G, Ferrari N, Santos S. Techno-economic evaluation of deploying CCS in SMR based merchant H_2 production with NG as feedstock and fuel. Energy Proc 2017;114:2690–712. doi:10.1016/j.egypro.2017.03.1533.

[10] Consonni S, Vigano F. Decarbonized hydrogen and electricity from natural gas. Int J Hydrogen Energy 2005;30:701–18. doi:10.1016/j.ijhydene.2004.07.001.

[11] Sanusi YS, Mokheimer EMA, Habib MA. Thermo-economic analysis of integrated membrane-SMR ITM-oxy-combustion hydrogen and power production plant. Appl Energy 2017;204:626–40. doi:10.1016/j.apenergy.2017.07.020.

[12] Sanusi YS, Mokheimer EMA. Thermo-economic optimization of hydrogen production in a membrane-SMR integrated to ITM-oxy-combustion plant using genetic algorithm. Appl Energy 2019;235:164–76. doi:10.1016/j.apenergy.2018.10.082.

[13] Martínez I, Romano MC, Fernández JR, Chiesa P, Murillo R, Abanades JC. Process design of a hydrogen production plant from natural gas with CO_2 capture based on a novel Ca/Cu chemical loop. Appl Energy 2014;114:192–208. doi:10.1016/j.apenergy.2013.09.026.

[14] Diglio G, Bareschino P, Mancusi E, Pepe F, Montagnaro F, Hanak DP, Manovic V. Feasibility of CaO/CuO/NiO sorption-enhanced steam methane reforming integrated with solid-oxide fuel cell for near-zero-CO_2 emissions cogeneration system. Appl Energy 2018;230:241–56. doi:10.1016/j.apenergy.2018.08.118.

[15] Akbari-Emadabadi S, Rahimpour MR, Hafizi A, Keshavarz P. Production of hydrogen-rich syngas using Zr modified Ca-Co bifunctional catalyst-sorbent in chemical looping steam methane reforming. Appl Energy 2017;206:51–62. doi:10.1016/j.apenergy.2017.08.174.

[16] Medrano JA, Potdar I, Melendez J, Spallina V, Pacheco-Tanaka DA, van Sint Annaland M, Gallucci F. The membrane-assisted chemical looping reforming concept for efficient H_2 production with inherent CO_2 capture: experimental demonstration and model validation. Appl Energy 2018;215:75–86. doi:10.1016/j.apenergy.2018.01.087.

[17] Herraiz L, Lucquiaud M, Chalmers H, Gibbins J. Sequential combustion in steam methane reformers for hydrogen and power production with CCUS in decarbonized industrial clusters. Front Energy Res 2020;8. doi:10.3389/fenrg.2020.00180.

[18] Wang F, Deng S, Zhang H, Wang J, Zhao J, Miao H, Yuan J, Yan J. A comprehensive review on high-temperature fuel cells with carbon capture. Appl Energy 2020;275:115342. doi:10.1016/j.apenergy.2020.115342.

[19] Winnick J, Toghiani H, Quattrone PD. Carbon dioxide concentration for manned spacecraft using a molten carbonate electrochemical cell. AIChE J 1982. doi:10.1002/aic.690280115.

[20] Sugiura K, Takei K, Tanimoto K, Miyazaki Y. The carbon dioxide concentrator by using MCFC. J Power Sources 2003;118:218–27. doi:10.1016/S0378-7753(03)00084-3.

[21] Lusardi M, Bosio B, Arato E. An example of innovative application in fuel cell system development: CO_2 segregation using molten carbonate fuel cells. J Power Sources 2004. doi:10.1016/j.jpowsour.2003.11.091.

[22] Milewski J, Bujalski W, Wołowicz M, Futyma K, Kucowski J, Bernat R. Experimental investigation of CO_2 separation from lignite flue gases by 100 cm^2 single molten carbonate fuel cell. Int J Hydrogen Energy 2014. doi:10.1016/j.ijhydene.2013.08.144.

[23] Rosen J, Geary T, Hilmi A, Blanco-Gutierrez R, Yuh C-Y, Pereira CS, Han L, Johnson RA, Willman CA, Ghezel-Ayagh H, Barckholtz TA. Molten carbonate fuel cell performance for CO_2 capture from natural gas combined cycle flue gas. J Electrochem Soc 2020;167:064505. doi:10.1149/1945-7111/ab7a9f.

[24] Manzolini G, Campanari S, Chiesa P, Giannotti A, Bedont P, Parodi F. CO_2 separation from combined cycles using molten carbonate fuel cells. J Fuel Cell Sci Technol 2012;9:011018. doi:10.1115/1.4005125.

[25] Campanari S, Chiesa P, Manzolini G. CO_2 capture from combined cycles integrated with molten carbonate fuel cells. Int J Greenh Gas Control 2010;4:441–51. doi:10.1016/j.ijggc.2009.11.007.

[26] Spinelli M, Campanari S, Consonni S, Romano MC, Kreutz T, Ghezel-Ayagh H, Jolly S. Molten carbonate fuel cells for retrofitting postcombustion CO_2 capture in coal and natural gas power plants. J Electrochem Energy Convers Storage 2018;15:031001. doi:10.1115/1.4038601.

[27] Spinelli M, Romano MC, Consonni S, Campanari S, Marchi M, Cinti G. Application of molten carbonate fuel cells in cement plants for CO_2 capture and clean power generation. Energy Proc 2014;63:6517–26. doi:10.1016/j.egypro.2014.11.687.

[28] Mastropasqua L, Pierangelo L, Spinelli M, Romano MC, Campanari S, Consonni S. Molten carbonate fuel cells retrofits for CO_2 capture and enhanced energy production in the steel industry. Int J Greenh Gas Control 2019;88:195–208. doi:10.1016/j.ijggc.2019.05.033.

[29] Margalef P, Brown TM, Brouwer J, Samuelsen S. Efficiency comparison of trigenerating HTFC to conventional hydrogen production technologies. Int J Hydrogen Energy 2012;37:9853–62. doi:10.1016/j.ijhydene.2012.03.099.

[30] Moradpoor I, Ebrahimi M. Thermo-environ analyses of a novel trigeneration cycle based on clean technologies of molten carbonate fuel cell, stirling engine and Kalina cycle. Energy 2019;185:1005–16. doi:10.1016/j.energy.2019.07.112.

[31] Mehrpooya M, Rahbari C, Moosavian SMA. Introducing a hybrid multi-generation fuel cell system, hydrogen production and cryogenic CO_2 capturing process. Chem. Eng. Process. - Process Intensif. 2017;120:134–47. doi:10.1016/j.cep.2017.07.008.

[32] Agll AAA, Hamad YM, Hamad TA, Thomas M, Bapat S, Martin KB, Sheffield JW. Study of a molten carbonate fuel cell combined heat, hydrogen and power system: energy analysis. Appl Therm Eng 2013;59:634–8. doi:10.1016/j.applthermaleng.2013.06.030.

[33] Li X, Ogden J, Yang C. Analysis of the design and economics of molten carbonate fuel cell tri-generation systems providing heat and power for commercial buildings and H_2 for FC vehicles. J Power Sources 2013;241:668–79. doi:10.1016/j.jpowsour.2013.04.068.

[34] Rinaldi G, McLarty D, Brouwer J, Lanzini A, Santarelli M. Study of CO_2 recovery in a carbonate fuel cell tri-generation plant. J Power Sources 2015;284:16–26. doi:10.1016/j.jpowsour.2015.02.147.

[35] Consonni S. Performance prediction of gas/steam cycles for power generation. Princeton University; 1992.

[36] GECOS, GECOS website, (2018). www.gecos.polimi.it (accessed April 2, 2019).

[37] FuelCell Energy, SureSource 1500 data sheet, 2017. https://www.fuelcellenergy.com/wp-content/uploads/2017/02/Product-Spec-SureSource-1500.pdf.

[38] Farooque M. The carbonate fuel cell-concept to reality. Wiley Interdiscip Rev Energy Environ 2015;4:178–88. doi:10.1002/wene.124.

[39] Park Y, Moon D-K, Kim Y-H, Ahn H, Lee C-H. Adsorption isotherms of CO_2, CO, N_2, CH_4, Ar and H_2 on activated carbon and zeolite LiX up to 1.0 MPa. Adsorption 2014;20:631–47. doi:10.1007/s10450-014-9608-x.

[40] Ma Z, Venkataraman R, Farooque M. High power internal-reforming direct carbonate fuel cell stack development through mathematical modeling and engineering optimization. J Fuel Cell Sci Technol 2010;7. doi:10.1115/1.4000625.

[41] Donazzi A, Beretta A, Groppi G, Forzatti P. Catalytic partial oxidation of methane over a 4% Rh/α-Al_2O_3 catalyst part I: kinetic study in annular reactor. J Catal 2008;255:241–58. doi:10.1016/j.jcat.2008.02.009.

[42] Chiesa P, Campanari S, Manzolini G. CO_2 cryogenic separation from combined cycles integrated with molten carbonate fuel cells. in. Int J Hydrogen Energy 2011:10355–65 Elsevier Ltd. doi:10.1016/j.ijhydene.2010.09.068.

[43] Campanari S, Chiesa P, Manzolini G, Bedogni S. Economic analysis of CO_2 capture from natural gas combined cycles using molten carbonate fuel cells. Appl Energy 2014;130:562–73. doi:10.1016/j.apenergy.2014.04.011.

[44] Mastropasqua L, Spinelli M, Paganoni A, Campanari S. Preliminary design of a MW-class demo system for CO_2 capture with MCFC in a university campus cogeneration plant. Energy Proc 2017;126:453–60. doi:10.1016/j.egypro.2017.08.213.

[45] Campanari S, Mastropasqua L, Gazzani M, Chiesa P, Romano MC. Predicting the ultimate potential of natural gas SOFC power cycles with CO_2 capture–part B: applications. J Power Sources 2016;325:194–208. doi:10.1016/j.jpowsour.2016.05.134.

[46] Berstad D, Anantharaman R, Nekså P. Low-temperature CO_2 capture technologies–applications and potential. Int J Refrig 2013;36:1403–16. doi:10.1016/j.ijrefrig.2013.03.017.

[47] NETL. *Seventh Edition Fuel Cell Handbook*. United States. doi:10.2172/834188. https://www.osti.gov/biblio/834188-seventh-edition-fuel-cell-handbook.

[48] Audasso E, Bosio B, Bove D, Arato E, Barckholtz T, Kiss G, Rosen J, Elsen H, Gutierrez RB, Han L, Geary T, Willman C, Hilmi A, Yuh CY, Ghezel-Ayagh H. New, dual-anion mechanism for molten carbonate fuel cells working as carbon capture devices. J Electrochem Soc 2020;167:084504. doi:10.1149/1945-7111/ab8979.